Nanoscale

REVIEW

View Article Online
View Journal | View Issue

Cite this: *Nanoscale*, 2025, **17**, 27762

Recent advances in carbon-based quantum dots for sensing applications

Shamim Ahmed Hira, Sharmila Durairaj, Carlos A. Ramirez and Aicheng Chen *

Carbon-based quantum dots (CQDs) are an emerging class of nanomaterials with unique features due to their quantum confinement effects. They have attracted tremendous attention due to several special features such as intrinsically low toxicity, high solubility in a variety of solvents, excellent biocompatibility, high specific surface area, abundant edge sites, and their capacity for easy modification with other nanomaterials. Due to these unique attributes, CQDs have been explored for numerous applications, including solar cells, energy storage, catalysis, drug and gene delivery, optoelectronics, sensors, and more. The quest for more sensitive electrodes consisting of cost-effective materials has led to the development of electrochemical sensors using CQDs for the detection of various analytes. In this review, the synthesis and characterization of CQDs are summarized and compared. The sensing applications of CQDs, encompassing biomarker detection, environmental monitoring, food safety and quality control, and the determination of pharmaceutical compounds are highlighted. Further, the challenges and future outlooks in CQDs research are briefly outlined.

Received 14th September 2025,
Accepted 9th November 2025

DOI: 10.1039/d5nr03879k

rsc.li/nanoscale

1. Introduction

Carbon-based quantum dots (CQDs) are a new type of zero-dimensional carbon-based nanomaterials (Ø < 10 nm) with distinct crystal formations and quantum confinement characteristics.[1] They can be applied across a broad range of domains in solar cells, energy storage, catalysis, drug delivery, gene delivery, optoelectronics, sensors, and more, due to their inherently low toxicity, high solubility in a variety of solvents, excellent biocompatibility, high specific surface areas, and numerous edge sites.[2–7] Due to the plethora of carboxyl groups on their surfaces, CQDs have great potential to either contain appropriate chemically reactive groups for functionalization or to connect with diverse polymeric, organic, biological, inorganic, or natural materials for surface modification. The passivation of their surfaces promotes fluorescence, while surface functionalization improves their solubility in both aqueous and non-aqueous media.[8] Abundant ambient oxygen environments can create new energy states within the band gaps of CQDs.[9] Contingent on the selected synthesis pathway, CQDs may be produced *via* "top-down" or "bottom-up" strategies as shown in Scheme 1.[10–18]

For this review article, we initially discuss the genesis and synthesis of CQDs, as their discovery and features have emerged *via* the culmination of several synthetic routes. Next, we set our focus on the applications of CQDs in the sensing domain over the last several years, where they have been integrated as key components under different principles and methods.[19,20] We also highlight the advantages of CQDs for sensing applications, which have been optimal in specific

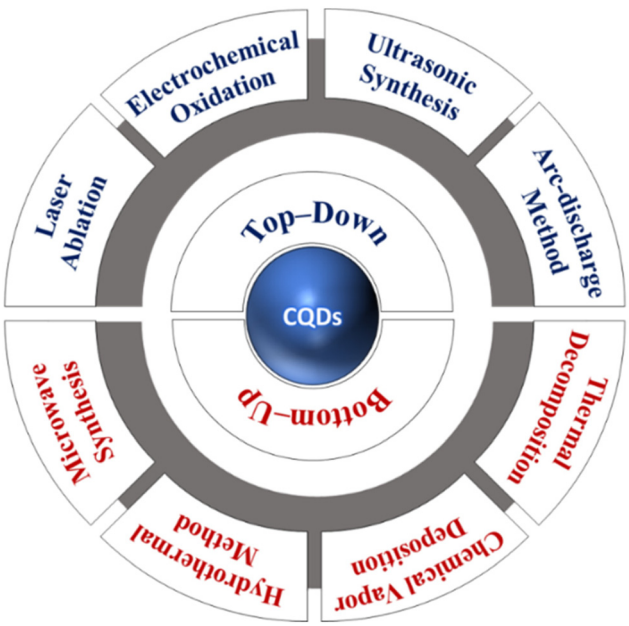

Scheme 1 Schematic of the synthesis of carbon-based quantum dots (CQDs) using "top-down" and "bottom-up" strategies.

Electrochemical Technology Centre, Department of Chemistry, University of Guelph, 50 Stone Road East, Guelph, Ontario N1G 2W1, Canada.
E-mail: aicheng@uoguelph.ca

fields. Furthermore, our discussion extends to describing potential future directions for CQD-based nanomaterials in various applications. Consequently, we trust that this review article will contribute and be of assistance to the growing scientific community that is engaged in CQD sensing, as well as medical and environmental applications.

2. Protocols for the synthesis of CQDs

Over the last few decades, several strategies have been proposed for the synthesis of CQDs with desired features. These methods are classified as two types: "top-down" and "bottom-up". For the top-down approach, bulk carbon materials such as carbon fibers, graphene, activated carbon, carbon soot, carbon black, and carbon nanotubes (CNTs) are converted to CQDs.[21–26] The processes employed for the top-down approach include electrochemical exfoliation/oxidation, oxidative acid treatment, laser ablation, arc discharge, *etc*.[27–30]

Harsh conditions may be required for some of the top-down techniques, which result in high costs. Conversely, for bottom-up approaches, the CQDs are prepared from carbon-containing materials through a "carbonization-decomposition-polymerization" process. Various natural materials such as polysaccharides,[31] carbohydrates,[32] biomass (*i.e.*, silk, betel nutshell, honey, orange juice, *etc*.),[33–37] synthetic polymers such as polythiophene,[38] polyethylene glycol (PEG),[39] or small organic molecules including amino acids, polyol, and citric acids can be selected as carbon sources.[40–44] Synthesis methods include hydrothermal methods, microwave assisted synthesis, ultrasonic irradiation, plasma treatments, *etc*.[45–50]

2.1. Top-down approach

2.1.1. Laser ablation. Laser ablation is a well-recognized technique for the fabrication of various nanostructures, where a laser is employed as an energy source to ablate solid target materials. Shen *et al.* fabricated N-doped CQDs using femtosecond laser ablation with graphene as the carbon source.[51] Due to the high peak power of femtosecond lasers, in contrast to other lasers, they can easily break chemical bonds. As CQDs have limited fluorescent features, ammonia was utilized as a dopant source to enhance their optical and electronic properties. The resulting as-prepared material may then be used in biomedical applications.[51] As a unique and promising synthesis route, laser ablation has been applied in the preparation of CQDs owing to the advantages of a short period and simple operation. However, several disadvantages constrain the laser ablation technique such as the slow rate of CQDs production and high cost of the required equipment.

2.1.2. Electrochemical oxidation. Electrochemical oxidation is an extensively utilized technique for the synthesis of CQDs using a bulk carbon precursor. Typically, two carbon-based electrodes are engaged in a water-based electrolyte. $OH^{\bullet}$ radicals may be generated by the applied electrode potential, which serve as "scissors" for the formation of CQDs.[55] During conventional electrochemical synthesis, controlling the dimensions of the CQD is challenging; thus, further processing is required to obtain a narrow size distribution. Nevertheless, monodispersed carbon-based nanomaterials can be synthesized by tuning parameters such as the starting material or applied potential. Ahirwar *et al.* reported on a strategy for the synthesis of monodispersed CQDs starting from low-molecular-weight alcohol.[52] Among the technologies commonly used to develop CQDs, electrochemical oxidation offers the following advantages: cost effectiveness, high purity, high yield, and controlled dimensions with good reproducibility. The possible drawback of this process is the creation of oxygen containing functional groups, which necessitated further operations to obtain pure CQDs.

2.1.3. Ultrasonic assisted synthesis. Nanomaterials may be synthesized using ultrasonic assisted synthesis under high temperatures and pressures with long reaction times. Several factors including dimensions, morphologies, chemical compositions, solubilities, surface structures, and aggregation capacities can be influenced *via* ultrasound. Qi *et al.* synthesized fluorescent N-doped CQDs (N-CQDs) using ultrasonic synthesis with a natural amino acid as a precursor, which were applied for cell imaging and optoelectronics.[53] The synthesized CQDs exhibited unexpected optical features including excellent photostability, strong photobleaching resistance, high quantum yields, *etc*., and demonstrated good results for cell imaging. Ultrasonic-assisted strategies have been acknowledged to possess the advantages of low cost and simple operation for the preparation of CQDs. Nevertheless, the main drawback for the synthesis of CQDs using this technique is the high energy cost.

2.1.4. Arc-discharge method. Fig. 1(A–C) depict the reaction pathways for the synthesis of CQDs and N-CQDs along with a schematic of the experimental setup used to synthesize CQDs through gas–liquid discharges in 1-butanol. The gas–liquid discharge process typically undergoes several stages, including ignition, mitigation, re-ignition, and ultimately extinction, waveforms of applied and discharge voltage, and the resulting discharge current.[54] Three types of carbon nanoparticles were obtained with different fluorescence features during the synthesis of SWCNTs. The as-prepared CQDs emitted yellow, orange, and blue-green fluorescence at ~365 nm. Additional characterization revealed hydrophilic carboxylic groups on the surfaces of the CQDs. The CQDs obtained by the arc-discharge method possessed high water solubility although they had a large particle size distribution due to their variable dimensions. The specific surface areas of the CQDs decreased for larger particle sizes, which translated to constraints on the reaction sites during electrocatalytic processes. An arc-discharge technique is used for the decomposition of a bulk carbon precursor to form carbon atoms, which has the major advantage that CQDs are formed through the purification of carbon nanotubes as the byproduct. This method has a few disadvantages such as complex compositions and low quantum yields.[55,56]

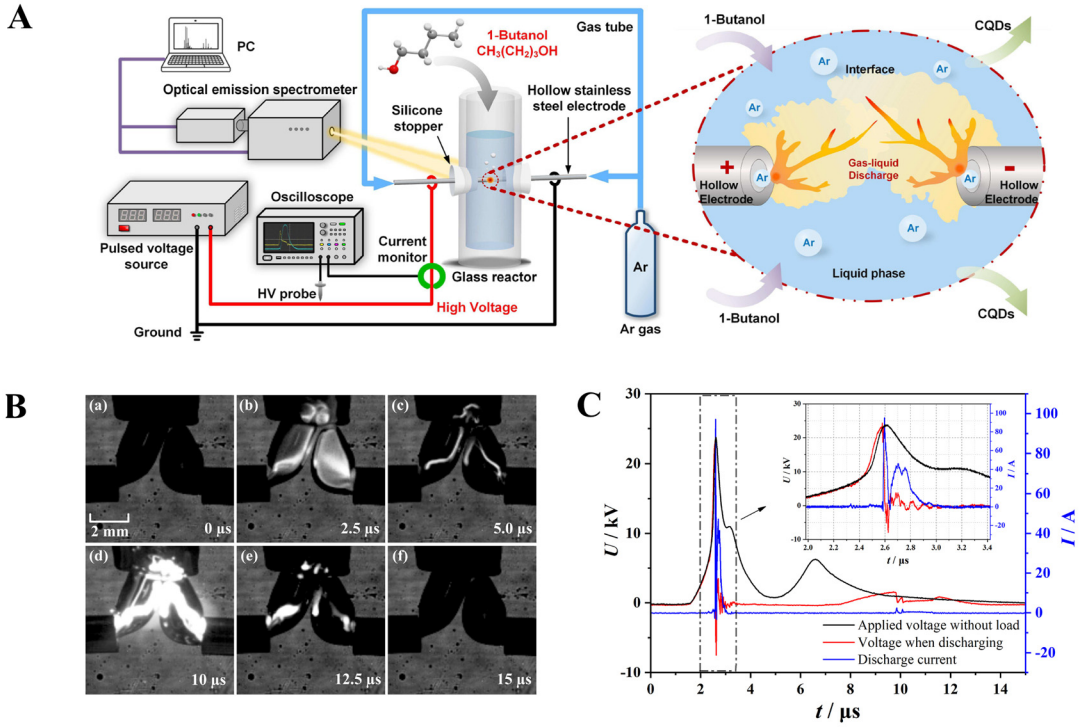

Fig. 1 Schematic of the synthesis of CQDs using the top-down approach: (A) Schematic diagram of experimental setup for synthesizing CQDs by gas–liquid discharges; (B) A typical evolution of gas–liquid discharge in 1-butanol. The discharge modes experience (b) ignition, (c) mitigation, (d) re-ignition and (e and f) extinction; (C) Waveforms of applied voltage, and discharge voltage and the resulting discharge current of arc discharge method. Reproduced with permission.[54] Copyright 2024, Elsevier.

2.2. Bottom-up approach

2.2.1. Microwave synthesis. Most of the approaches employed for the synthesis of CQDs are time-consuming and require complex instrumentation. However, there are facile and rapid strategies for the mass synthesis of CQDs (*e.g.*, microwave assisted techniques, where heating can be homogeneously applied). Fig. 2A shows a schematic for the synthesis of CQDs using a microwave assisted method. Nazar *et al.*[57] proposed a simple and economical microwave assisted technique for the synthesis of CQDs using Arabica coffee grounds. Subsequently, many researchers have sought to ameliorate this

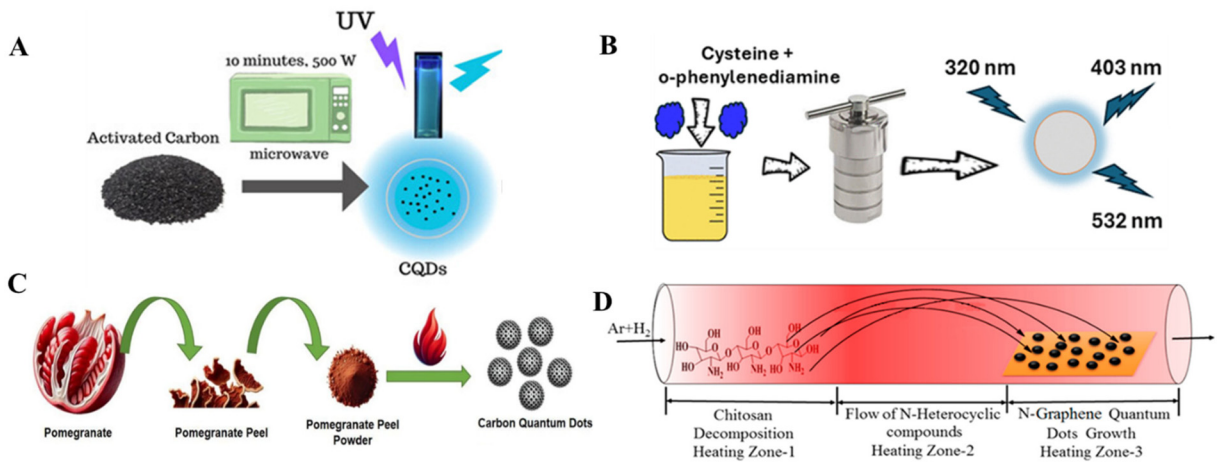

Fig. 2 Schematic for the synthesis of CQDs using the bottom-up approach: (A) microwave synthesis. Reproduced with permission.[57] Copyright 2024, American Chemical Society; (B) hydrothermal technique. Reproduced with permission.[59] Copyright 2025, Royal Society of Chemistry; (C) thermal decomposition. Reproduced with permission.[60] Copyright 2025, Elsevier; and (D) chemical vapor deposition. Reproduced with permission.[61] Copyright 2018, American Chemical Society.

process. For example, an ultrafast technique was developed by Li *et al.*, where CQDs with high quantum yields were synthesized using microwave irradiation within a few minutes.[58] The as-synthesized materials were utilized in light-emitting diodes and for cell imaging, with good performance being obtained in both cases. This technique has several benefits, including ease of use, solvent-free synthesis, precursor tolerance, fast reaction times and low cost. However, there are certain disadvantages for the microwave method (*e.g.*, large-scale reactions are not possible and separation and purification may be difficult).

2.2.2. Hydrothermal technique. The hydrothermal approach is a convenient process that is extensively used for the synthesis of carbon-containing materials. Fig. 2B displays a schematic for the synthesis of CQDs using the hydrothermal method. It is a non-toxic, cost-effective, and eco-friendly technique for which several precursors such as chitosan,[62] glucose,[63] citric acid,[64] orange juice,[65] banana juice,[66] and sucrose[67] may be used. The organic precursor in an aqueous solution is sealed in a hydrothermal vessel, and the reaction is performed under high temperatures. The reaction temperature and time are the essential parameters, which may influence the optical features of the synthesized carbon-based nanomaterials.[68] Using the hydrothermal method, Ali *et al.* synthesized a nitrogen and sulfur-doped dual-emission carbon dot (NSDC-dots)-based fluorescence sensor for the determination of cobalt and aluminum ions in canned food products.[59] In another work, Halder *et al.* reported on the one-pot synthesis of CQDs using graphene oxide (GO) as a precursor and obtained interesting results in cell uptake studies.[69] This method is environmentally benign, non-toxic, and cost-effective. Nevertheless, a disadvantage of this technique is that it contains impurities such as larger and undissolved particles.

2.2.3. Thermal decomposition. Thermal decomposition or pyrolysis is an effective method for the preparation of CQDs, where macroscopic carbon structures are used as precursors. Fig. 2C displays a scheme reported by Huang *et al.* to illustrate the fabrication of CQDs from pomegranate peel using the thermal decomposition method.[60] This technique is advantageous in terms of rapid reaction times, low cost, solvent-free reactions, as well as less complex instrumentation, *etc*. Higher acidic or alkaline concentrations are employed to disassociate the carbon precursor into carbon particles. Ma *et al.* synthesized N-doped CQDs by carbonizing ethylene diamine tetra acetic acid under high temperatures.[70] The use of renewable resources together with the facile thermal decomposition method is promising for the sustainable and cost-effective synthesis of CQDs for practical applications. This strategy has some demerits including that it involves a prolonged synthesis process and the removal of impurities may be problematic.

2.2.4. Chemical vapor deposition. Chemical vapor deposition (CVD) is a well-established technique that has been employed over the last few years for the synthesis of CQDs. Fig. 2D shows a schematic of the CVD method for the synthesis of CQDs. Using the CVD technique, it is possible to control the dimensions of the CQDs by varying the parameters such as the growth time, carbon source, substrate temperature, and carrier gas flow rate. Fan *et al.* introduced a CVD technique for the synthesis of CQDs using methane as the carbon source,[71] where alcohol and HCl were used to clean a copper foil substrate, which was then heated under a mixture of Ar and H_2. Kumar *et al.* synthesized N-doped CQDs utilizing chitosan as a carbon source *via* the CVD method.[61] The CVD method offers several advantages such as operating at a lower temperature range, relatively high purity, and the ease of scaling up reactions. The main drawback of this technique is it requires highly expensive instrumentation.

3. Applications of CQDs in sensing

The various unique physicochemical attributes of CQDs and potential for the synthesis of a large panel of carbon-based nanostructures have made them of intense interest for applications in diverse fields, ranging from sensors and catalysis to energy and medicine. Over the years, CQDs based sensors have gained tremendous attention due to some of their unique physical, chemical and electrochemical properties.[72] Here, we highlight some of the promising sensing applications of CQDs in domains such as (i) biomarker detection, (ii) environmental monitoring, (iii) food safety, and (iv) detection of pharmaceutical compounds.

3.1. Biomarker detection

According to the World Health Organization (WHO), biomarkers may be defined as substances, structures, or processes whose presence indicate diseases, infections, or any deleterious environmental exposures.[73] These might include proteins, genes, lipids, and metabolites that normally exist in serum, as well as tumor tissues, and body fluids (*e.g.*, saliva, blood, urine, sweat). Biomarkers can differentiate between normal and abnormal physiological states, where earlier detection may increase therapeutic success rates.[74–77] Consequently, it is critical to synthesize functional materials that can be utilized for their detection. In this section, we discuss the application of CQD-based sensors for the recognition of different types of biomarkers, including cardiac, cancer, protein, stress biomarkers, *etc*.

3.1.1. Detection of cardiac biomarkers. Cardiovascular diseases related to heart and blood vessels comprise ~33% of deaths on a global scale.[78] Individuals who are at higher risk for cardiovascular conditions may reveal symptoms such as increased glucose levels, higher blood cholesterol, high blood pressure, and increasing body weight, which are for the most part monitored in healthcare centers. It is essential to diagnose these patients at early stages. Consequently, more attention has been given to minimizing the risks of cardiovascular disease using standard biomarkers. Previously, numerous nanomaterial-based electrodes have been prepared for use as electrochemical sensors.[79] CQDs and gold nanoparticles (AuNPs) have garnered significant interest toward the development of electrochemical immunosensors.

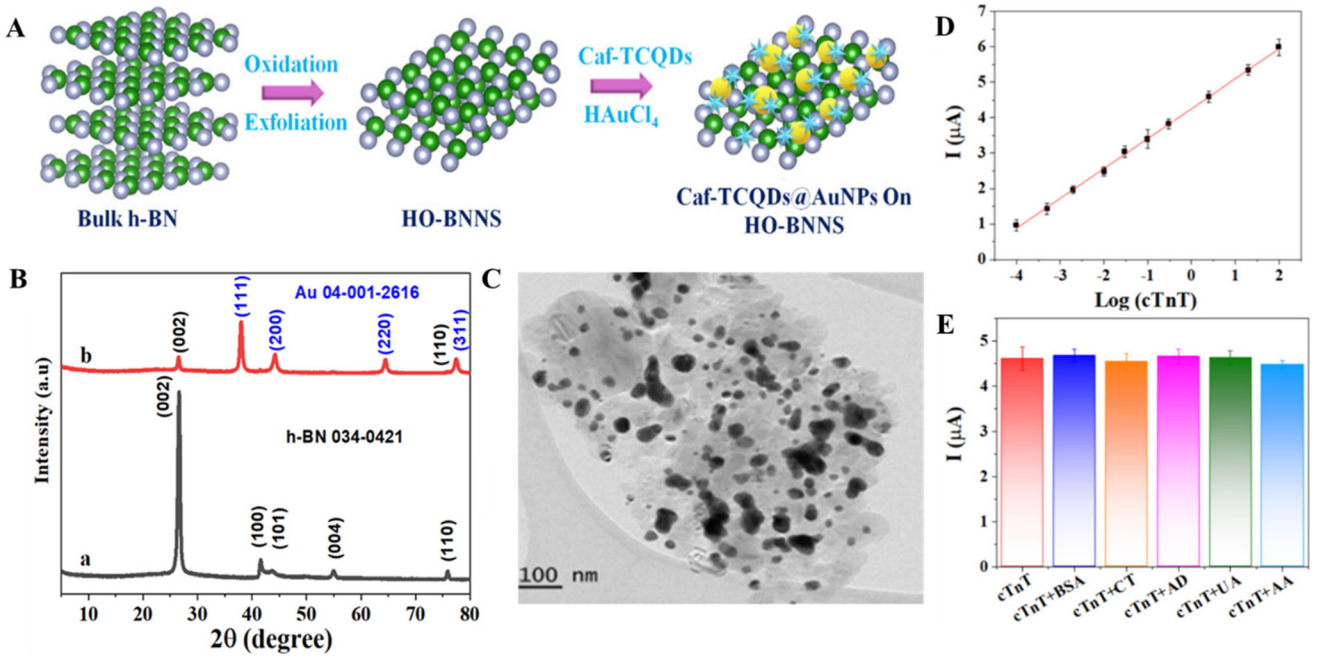

Fig. 3 (A) Schematic representation of the preparation process for caf-TCQDs@AuNPs on HO-BNNS; (B) XRD patterns HO-BNNS (black) and caf-TCQDs@AuNPs on HO-BNNS (red); (C) TEM image of caf-TCQDs@AuNPs on HO-BNNS; (D) Calibration curve of cTnT over 0.0001 to 100 ng mL^{-1}; (E) DPV current response of the immunosensor after incubation with 10 ng mL^{-1} cTnT in the absence and the presence of other interference analogs. Reproduced with permission.[80] Copyright 2024, American Chemical Society.

Kim *et al.* developed an immunosensor for the detection of cardiac troponin T (cTnT),[80] consisting of a composite made up of highly water-soluble hydroxylated boron nitride nanosheets (HO-BNNS) and carboxyl-terminated triangular CQDs (caf-TCQDs), in conjunction with AuNPs. A schematic for the synthesis of the caf-TCQDs@AuNPs on HO-BNNS is shown in Fig. 3A. Following the decoration of caf-TCQDs@AuNPs on HO-BNNSs, four distinct peaks were observed at 2θ values of 37.9°, 44.1°, 64.4°, and 77.3° (Fig. 3B). These peaks correspond to the standard Bragg reflections (111), (200), (220), and (311) of a face-centered cubic (fcc) lattice structure of AuNPs. TEM image (Fig. 3C) reveals that caf-TCQDs@AuNPs was successfully anchored to HO-BNNS. A linear correlation was observed between the electrochemical current and the logarithmic cTnT concentration (Fig. 3D). The limit of detection achieved in this study was 0.0013 ng mL^{-1}. To assess the selectivity of the developed immunosensor, the electrochemical responses to 10 ng mL^{-1} cTnT in the absence and the presence of potential interfering species such as creatine (CT), bovine serum albumin (BSA), avidin (AD), ascorbic acid (AA), and uric acid (UA) were measured (Fig. 3E). No notable changes of the current response were observed, showing the high selectivity of the immunosensor for the detection of cTnT.

3.1.2. Detection of cancer biomarkers. Cancer is a global health issue that has emerged as a serious concern in the modern world. Due to its widespread occurrence, early detection and appropriate treatment strategies are essential.[81] Currently, low- and middle-income countries are critically affected due to the high cost and lack of accurate and early determination of cancer biomarkers. As a result, the cure rate for cancer is lagging and is a significant strain on society.[82] Researchers are attempting to identify suitable nanomaterials for the early detection of cancer. For example, Xi *et al.* prepared an N-doped CQD/N-doped carbon hollow sphere nanomaterial composite for the early detection of cancer biomarkers.[83] Kurniawan developed a tunable CQD for the sensitive and selective detection of cancer biomarkers.[84] Dutta *et al.* fabricated an immunosensor using nitrogen-doped graphene quantum dots (GQDs) and single-walled carbon nanohorns (SWCNHs) for the sensitive determination of a common cancer biomarker (alpha-fetoprotein (AFP)) as illustrated in Fig. 4.[85] Fig. 4A depicts the fabrication of N-GQD. An electrode material known as N-GQD@SWCNHs was utilized to detect a cancer biomarker. A GCE/N-GQD@SWCNHs/Anti-AFP/BSA immunosensor was created through the application of a uniform layer of a bioconjugate dispersion (N-GQD@SWCNHs/Anti-AFP) onto a glassy carbon electrode (GCE) surface. Subsequently, BSA was used to block the remaining active sites to prevent nonspecific adsorption (Fig. 4B and C). Fig. 4D portrays the CVs of the prepared immunosensor for the detection of various concentrations (0 ng mL^{-1} to 200 ng mL^{-1}) of α-fetoprotein (AFP). With increasing concentrations of the antigen (AFP), a gradual decline in the cathodic peak current and a gradual rise in anodic peak current were observed (Fig. 4E). The immunosensor demonstrated a wide dynamic range (0.001 ng mL^{-1} to 200 ng mL^{-1}) with a detection limit of 0.25 pg mL^{-1} at a signal-to-noise ratio of S/N = 3.

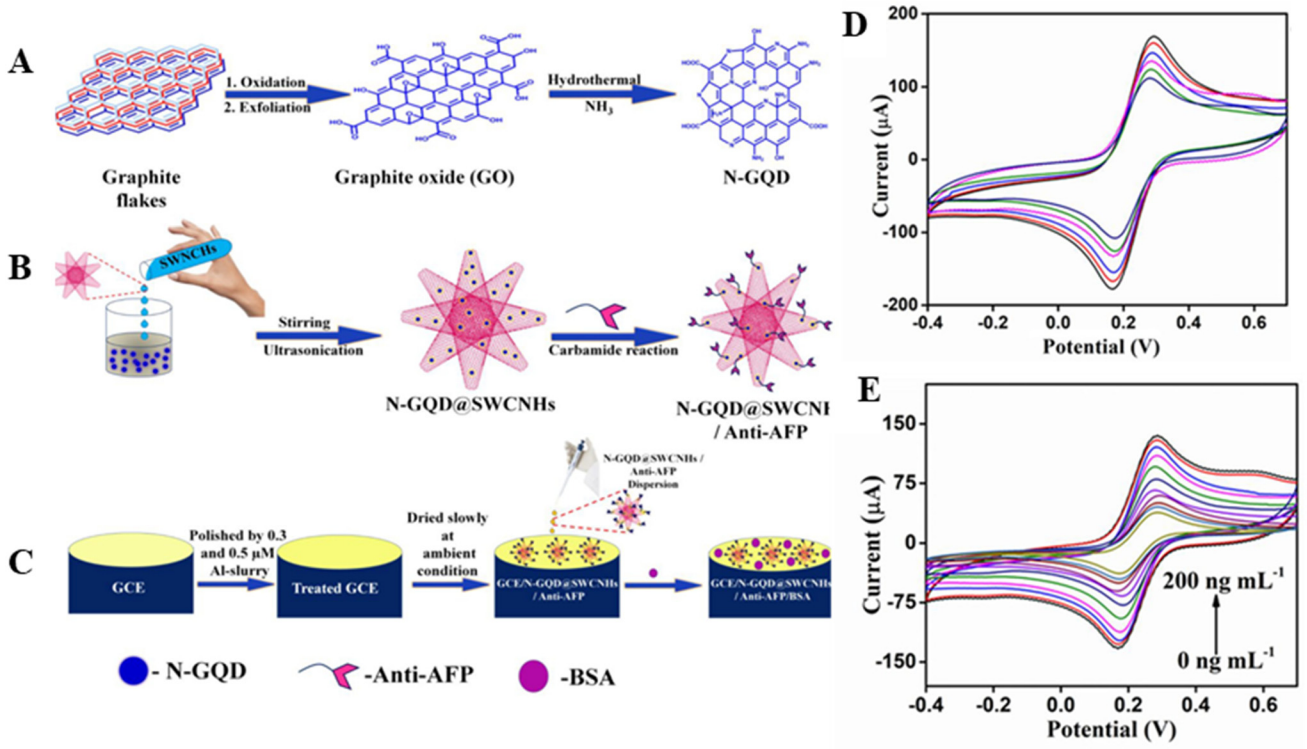

Fig. 4 (A) Synthesis of N-GQD using graphite flakes as a starting material; (B) synthesis of the nanocomposite and anti-AFP incorporated bioconjugates; (C) the fabrication process of the immunosensor; (D) CVs GCE/N-GQD@SWCNHs/Anti-AFP/BSA with different concentrations of AFP antigen (from outer to inner curve: 0, 0.001, 0.01, 0.1, 1, 10, 60, 100, 150, 175, and 200 ng mL^{-1}, respectively); (E) dependence of peak current on logarithm of the AFP concentration. Reproduced with permission.[85] Copyright 2021, American Chemical Society.

3.1.3. Detection of protein biomarkers. C-reactive protein (CRP) is an inflammation biomarker related to atherosclerosis, incident myocardial infarction, peripheral arterial diseases, and sudden cardiac death.[86] Concentrations of CRP in the ranges of 3–10, 1–3, and <1 mg L^{-1} represent high, medium, and low risks of having cardiovascular disease; thus, it is essential to develop an immunosensor for the sensitive and precise detection of CRP. Korram *et al.* reported on onion-derived carbon dots (OCDs) for the detection of prostate specific antigen (PSA).[87] The inset of Fig. 5A shows an HRTEM image (fringes image) of the prepared OCDs, which exhibited a *d*-spacing of 0.34 nm. The inset of Fig. 5A shows a lattice fringe image with a *d*-spacing of ~0.33 nm, which is consistent with the (0 0 2) facet of graphitic carbon. Fig. 5B shows that OCDs presented a size range of 2–6.32 nm with an average diameter of 3.38 nm. Fig. 5C reveals the excitation-dependant emission behaviour of OCDs, which may be associated with the surface states that affect the band gap.[88] Fig. 5D shows a schematic for the construction of a sandwich immunosensor for the detection of PSA, illustrating signal amplification by the OCDs during an electrochemical immunoassay. The current response of the immunosensor was significantly enhanced with increased concentrations of PSA (Fig. 5E). Within the concentration range of 0.1–100 ng ml^{-1}, the PSA was proportional to the aerometric current response (Fig. 5F). Hennessey *et al.*[89] proposed a novel type of antibody (a-CRP) to identify the special interactions between CRP and a-CRP, while the efficacy of this technique was explored using different CRP concentrations. In another study, Kokkinos *et al.* reported on a sensor that utilized QDs based on bismuth citrate-modified graphite (SPEs),[90] where a low limit of detection (0.05 ng mL^{-1}) and a wide linear range (0.2 to 100 ng mL^{-1}) were achieved.

3.1.4. Oxidative stress biomarkers. Several biomarkers have been recognized as an indicative of oxidative stress (*e.g.*, glutathione, nitrogen dioxide, hydrogen peroxide, ferritin, nitrotyrosine, carboxymethyl-lysine (CML), 4-nitroquinoline N-oxide (4-NQO)). CML is a type of advanced glycation end-product (AGE) that functions as an active element of harmful metabolites in diabetes mellitus. CML arises from the thermal processing of food, the oxidation of fructose-lysine within the glycolytic pathway, and the interaction of lysine with lipid peroxidation and amino acids in the advanced lipid peroxidation end-product (ALE) pathway. Kumar *et al.* described a CQD-based immunosensor for the detection of CML.[91] The CQDs were synthesized from dried orange peel using a hydrothermal method (Fig. 6A). The fabrication of the immunosensor is illustrated in Fig. 6B. The carbon dots exhibited an optical absorption peak in the ultraviolet (UV) region (286 nm), with a tail reaching into the visible spectrum (Fig. 6C). Differential Pulse Voltammetry (DPV) technique was utilized for the electrochemical detection, where the current response

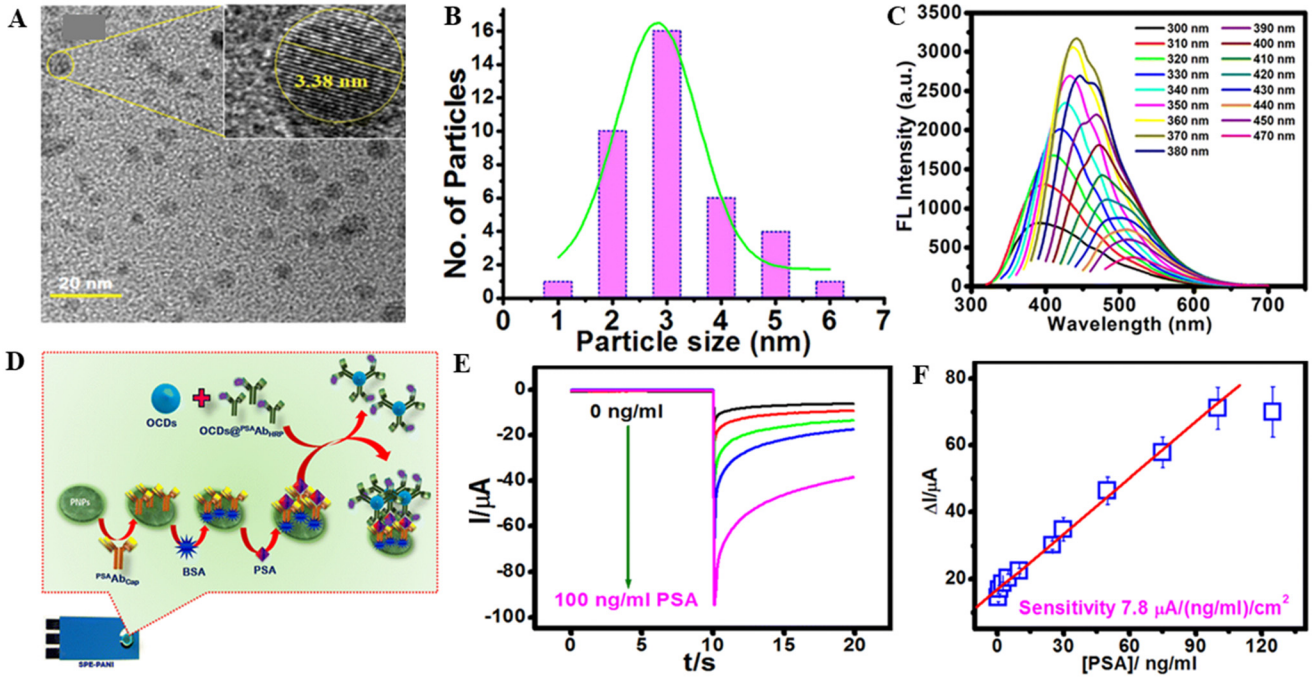

Fig. 5 (A) TEM image and magnified image of HRTEM (inset), (B) the size distribution histogram of OCDs; (C) FL spectra of OCDs excited at different wavelengths ranging from 300 nm to 470 nm; (D) schematic representation of OCDs-based immunosensor for the detection of PSA; (E) Amperometric curves of OCD@$^{PSA}Ab_2$ detection probe-based PSA biosensor in the presence of 3 mM HQ and 4.5 mM H_2O_2 at different concentrations of PSA; (F) the calibration plot for the OCD@$^{PSA}Ab_{HRP}$-based PSA biosensor. Reproduced with permission.[87] Copyright 2025, Royal Society of Chemistry.

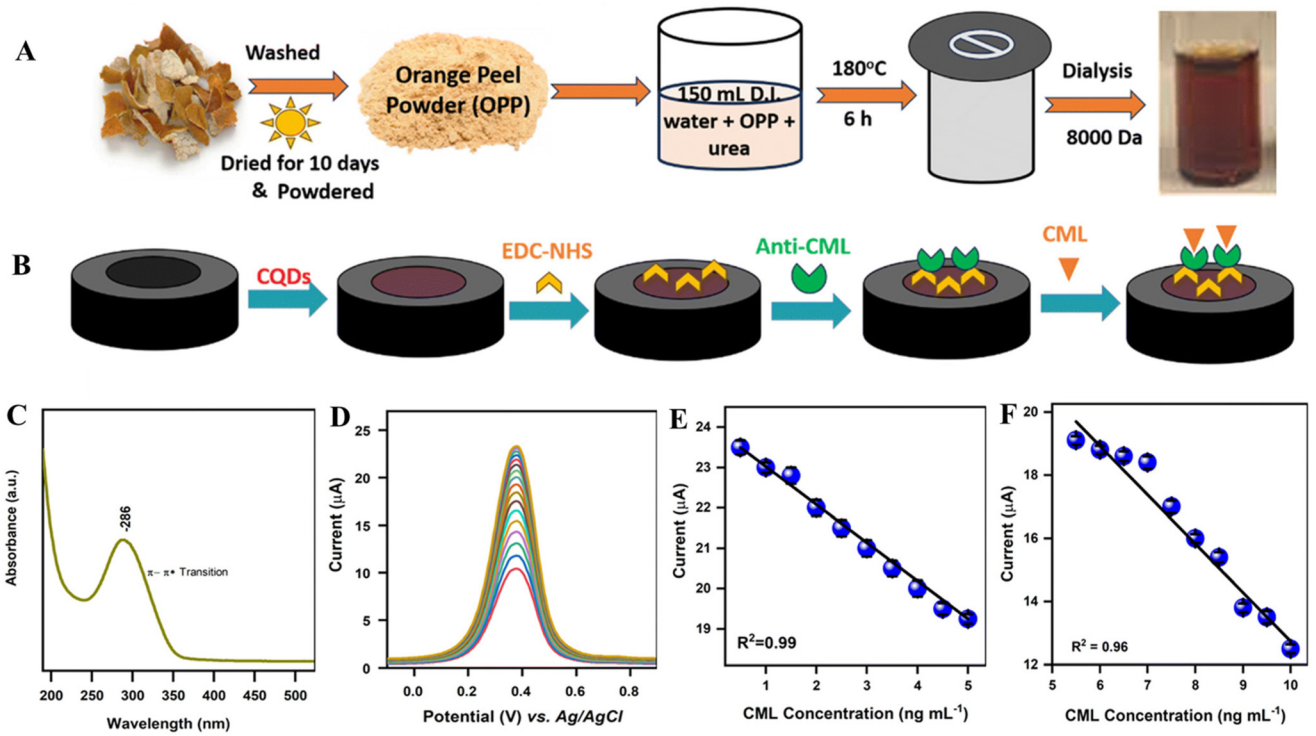

Fig. 6 (A) Schematic representation for the CQDs; (B) fabrication of the working electrode using CQDs; (C) UV-vis spectrum of CQDs; (D) DPV of the CQDs/anti-CML/EDC-NHS modified GC electrodes in the presence of CML; linear calibration curve for increasing CML concentrations of (E) 0.5–5.0; (F) 5.5–10.0 ng mL^{-1} with adjusted regression coefficients of R^2 = 0.99 and 0.96, respectively. Reproduced with permission.[91] Copyright 2025, Royal Society of Chemistry.

decreased with higher CML concentrations (Fig. 6D). This was due to the formation of immunological complexes. As illustrated in Fig. 6E and F, the developed biosensor demonstrated two separate linear concentration ranges: 0.5–5 ng mL^{-1} and 5–10 ng mL^{-1}, with the detection limit being 0.027 ng mL^{-1}.

Glutathione is another oxidative stress biomarker, which is a non-protein thiol-based compound. It exists not only in mammalian tissues, but also in different plants, and plays significant roles in biological cycles such as xenobiotic metabolism, gene regulation, intracellular redox activities, *etc*. Anomalous glutathione levels may induce several health issues such as heart problems, cancer, aging, and other difficulties. Thus, it is necessary to develop an effective means for the determination of glutathione. Liu *et al.* reported on DA-modified N-doped GQDs for the efficacious determination of glutathione.[92] Human urine and serum media were utilized to test the practical applicability of the fabricated sensor with good recovery (96–103%).

4-nitroquinoline N-oxide (4-NQO) is a vital stress biomarker generated by cancer cells that is linked to nucleotide excision repair, where abnormal levels may induce distinct carcinogenic diseases. Thus, it is important to develop simple, reliable, and sensitive strategies for the rapid detection of 4-NOQ. Muthumariyappan *et al.* synthesized Bi_2WO_6/rGOS nanocomposites for the selective and sensitive determination of 4-NOQ.[93] The practical applicability of the sensor was determined using human blood and urine as real samples with satisfactory recoveries. Li *et al.* described nanoporous gold-chitosan hybrids and GQD functionalized Au@Pt electrodes for the electrochemical detection of carcinoembryonic antigen (CEA) for which a low limit of detection was obtained with high sensitivity.[94] In another work, Jang *et al.* reported on a Nafion coated Au nanoparticle-GQD nanocomposite electrode for the sensitive recognition of dopamine.[95] Moreover, Aoun *et al.* synthesized and employed an N-doped GQD-chitosan based composite material for the sensitive electrochemical detection of dopamine.[96] There are also several reports on CQD- and GQD-based materials for the electrochemical detection of different stress biomarkers such as epinephrine, serotonin, norepinephrine *etc*., which exhibited low limits of detection and high sensitivities.[97–103]

3.2. Environmental monitoring

Clean air, pure water, fresh food, and a clean environment are fundamental for human survival and critical for human socio-economic development. Demands for the production of many products have led to serious environmental threats; thus, it is important to identify alternative solutions to reduce environmental risks.[104,105] Herein, we discuss the application of CQD-based nanomaterials for the assessment of potential environmental risks, which have been categorized as: (i) heavy metal ion detection, and (ii) determination of toxic compounds.

3.2.1. Heavy metal ion detection. Even though some elementals such as zinc (Zn), copper (Cu), manganese (Mn), *etc*. are crucial for human health; others such as cadmium (Cd), mercury (Hg), arsenic (As), chromium (Cr), and lead (Pb) are highly toxic. The latter can induce severe deleterious effects in mammals and may create serious environmental contamination. Heavy metals from myriad sources are released into oceans, rivers, lakes, and canals, which pollute the environment. Abnormal heavy metal levels not only hinder crop growth and their yields but also have harmful impacts on the central nervous systems and digestion of mammals. The consumption of heavy metal-laced shellfish, fish, rice, wheat, *etc*. by humans can result in heavy metal poisoning. The direct analysis of ultralow concentrations of chemical species in complex samples is quite challenging, where sophisticated equipment and critical time-consuming separations are some of the disadvantages. Therefore, it is vital to develop strategies for the direct detection of small analytes in complex samples. Lu *et al.* proposed an ultrasensitive technique for the detection of small analytes such as Cu^{2+}, Hg^{2+}, and Cd^{2+} in a complex sample using an ordered mesoporous silica-nanochannel film (VMSF) loaded with GQDs.[106] The limits of detection obtained for Hg^{2+}, Cd^{2+}, and Cu^{2+} were 9.8 pM, 4.3 pM, and 8.3 pM, respectively.

Tian *et al.* developed a fluorescent nanosensor for heavy metal detection based on CQDs enhanced by machine learning.[107] Fig. 7A shows the synthesis and detection methods of the CQDs, their characterization with TEM and fluorescence, and responses to different concentrations of Cu^{2+}, as well as a machine learning technique and Z-score analysis to determine concentrations close to the LOD. This machine learning-enhanced fluorescent nanosensor improved the LODs by using a K-nearest neighbors (KNN) model for Cu^{2+} (95 μM to 100 pM), Pb^{2+} (1012 μM to 10 nM), Fe^{3+} (3.5 μM to 100 pM), Hg^{2+} (900 μM to 10 nM), and Cr^{6+} (15 μM to 10 nM).[107] Fig. 7B illustrates a thin-film-based CQDs sensor for the detection of heavy metals in water matrices; an experimental procedure for the detection of heavy metal ions; the quenching mechanism, and its sensitivity to various ions.[108] The thin-film based CQDs sensor was developed by synthesizing the CQDs from folic acid, mixing them with a PVA heated solution and allowing them to cool in petri plates for the formation of thin films. The detection method consisted of a fluorescence-based mechanism and a fiber optic spectrometer device. The LODs for various heavy metals were found to range from 0.019–0.006 ppm. The capacity of this sensor to precisely detect heavy metal counts in tap, river, and ground water supplies, and its analytical parameters were compared with micro plasma-atomic emission spectroscopy.[108] Fu *et al.* developed N-GQDs for the sensitive and selective detection of toxic mercury ions,[109] where cyclic voltammetry (CV) and electrochemical impedance spectroscopy (EIS) techniques were used for sensing. The LOD for the detection of Hg^{2+} was 10 ppb, and the required accumulation time was 32 s. Ting *et al.* developed a sensor based on Au nanoparticle functionalized GQDs for the sensitive detection of Hg^{2+} and Cu^{2+},[110] which exhibited higher sensitivities and lower LODs in both cases.

3.2.2. Determination of toxic phenolic compounds. Phenolic compounds (*e.g.*, 4-nitrophenol, 2-nitrophenol, 2,4-dinitrophenol, bisphenol, *etc*.) are frequently employed in

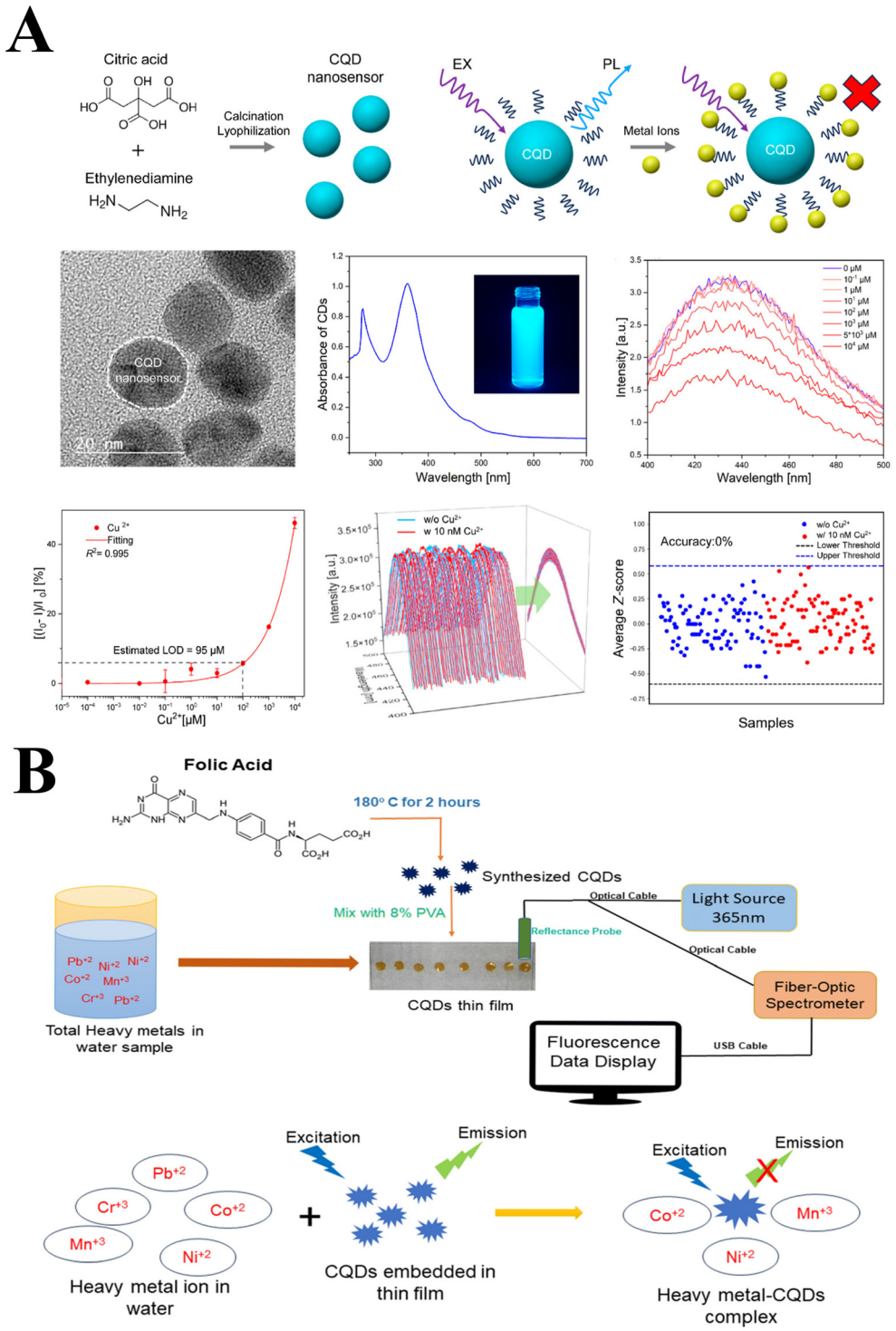

Fig. 7 (A) Synthesis and schematic diagram of the CQD nano sensor with the TEM image, UV-vis spectrum, fluorescence spectrum of the response to Cu^{2+}, calibration curve of the response to Cu^{2+}, overlapping of normal and analyte nano sensor spectrum, and average *Z*-score of normal and analyte nano sensor spectrum. Reproduced with permission.[107] Copyright 2024, American Chemical Society. (B) Schematic diagram of the experimental procedure for the detection of heavy metal counts, quenching mechanism of the synthesized CQDs thin film in the presence of heavy metal ions, and sensitivity of different heavy metal ions to this sensing mechanism. Reproduced with permission.[108] Copyright 2024, Royal Society of Chemistry.

various industrial and pharmaceutical processes; however, they are toxic to humans and animals. Among these compounds, 4-nitrophenol has been deemed the most toxic by the United States Environmental Protection Agency (USEPA). Consequently, it is desirable to develop effective strategies for the sensitive detection of 4-NP. Hira *et al.* fabricated a reliable electrochemical sensor for the detection of 4-NP.[111] The sensor exhibited low limits of detection and high sensitivity. In another work, they reported on Ag NPs deposited on metal tungsten bronze, which was applied for the reduction of 4-NP.[112] Recently, Das *et al.* fabricated N-doped CDs using ethylene glycol and β-Alanine for the detection of 4-NP using photoluminescence (PL) quenching.[113] The selective recognition of 2,4-dinitrophenol (2,4-DNP) in water was achieved by Chen *et al.* based on cucurbit[6]uril/*p*-aminobenzene sulfonamide CQDs (Q[6]-CQDs) using a one-step hydrothermal method (Fig. 8A).[114] The Q[6]-CQDs recognized the 2,4-DNP through changes in their fluorescence (Fig. 8B), where the titration fluorescence spectra of different concentrations of 2,4-DNP can be seen, as well as the respective calibration curve in Fig. 8C. The LOD was 0.15 μM, which made this sensor suitable for the detection of 2,4-DNP in aqueous media and contaminated water.[114] Fig. 8D reveals the fabrication of a PEDOT/CFP electrode modified with biomass-derived S-CQDs through electro-polymerization for the electrochemical detection of phloroglucinol.[115] DPVs for the oxidation of phloroglucinol at different concentrations were measured using the S-QCD + PEDOT/CFP electrode (Fig. 8E), with its associated calibration curve (Fig. 8F). The electrochemical sensor exhibited excellent electrocatalytic activities, low chemical impedance, and large specific surface area, as well as an LOD of 11 nM and the successful detection of phloroglucinol in industrial effluents.[115] Li *et al.* reported on chromium(III)-doped quantum dots for the determination of *p*-nitrophenol,[116] while Mehta *et al.* fabricated a GQD-modified screen-printed electrode for the sensitive electrochemical detection of parathion.[117] Hadidi *et al.* worked on a penicillamine-functionalized GQD-based electrode for the electrochemical detection of lead.[118] Cai *et al.* reported on a N-doped GQD-based nanomaterial for the electrochemical detection of 2,4,6-trinitrotoluene (TNT) with high sensitivity and good selectivity.[119]

3.3. Food safety

Since food is indispensable for sustaining life, food safety is a fundamental human need. Secure food supplies improve human health and extend longevity. The responsibility of the food chain begins at the farm and ends at the fork/plate, to negate any contamination by bacteria, hormones, and numerous other factors, which causes a wide range of poisoning and other major health risks for increasing numbers of people each year. Furthermore, contaminants such as antibiotic and pesticide residues pose serious threats to food safety.[120] Contaminated foods may also be potent vectors for the propagation of viruses, which can wreak havoc on global health and financial systems. For example, SARS-CoV-2 might be spread through contaminated seafoods to cause unprecedented global outbreaks. In consideration of these various issues, there is an urgent need for rapid and feasible food quality analysis over conventional methods. Over the last few decades, due to the development of nanotechnology, nanomaterials are leading the way toward addressing many challenges in the food safety sector. CQDs are one of the most promising and cost-effective sensor materials, which exhibit interesting sensing and biosensing applications including electrochemistry, fluorescence, and chemiluminescence.[121,122]

3.3.1. Metal contamination. CQDs and their abundant surface oxygen-based groups (*e.g.*, carbonyl, carboxyl, and hydroxyl) possess luminescence attributes that facilitate the emission of photoexcited electrons. Another notable fact is that doping with different halogens can create additional defects in the surfaces of the CQDs to enhance their optical, electrochemical, and fluorescent properties.[123] Metals such as copper, iron, and zinc are cofactors in various enzymes that are involved in multiple biological functions. Increased or decreased concentrations of metal ions can initiate health issues in living organisms. Thus, practicable and facile techniques need to be developed for the quantification of metal ions in ambient environments. CQDs synthesized from activated carbon through the oxidation of nitric acid is highly selective for the detection of Cu(II). When Cu(II) ions are added, the further quenching of fluorescence occurs, which is reinstated with the addition of oxalate. This response of Cu(II) to oxalate facilitates the quantification of Cu(II) in water samples.[124] Liu *et al.* synthesized CQDs using bamboo leaves, which were utilized for the detection of Cu^{2+} ions in river water samples, with an LOD of 115 nM and linear range from 0.333 to 66.6 μM, which confirmed their efficacy for the analysis of environmental water samples.[125] Yang *et al.* employed a one-step hydrothermal process to synthesize Zn-passivated CQDs (Z-CQDs), which were employed to detect EDTA and Zn^{2+}. Two detection mechanisms were identified: (i) EDTA-Zn^{2+} complexation reaction, and (ii) depassivation and passivation of Z-CQDs. The EDTA and Zn^{2+} detection concentrations varied from 2.5–25 μM and 2–15 μM, respectively, with detection limits of 0.3 μM and 0.5 μM, respectively. Subsequently, the sensor was used to determine the presence of EDTA and Zn^{2+} in tap water.[126] Wang *et al.* performed a one-step hydrothermal process with thymidine as a carbon source to synthesize a fluorescent sensor for the sensitive detection of Cr^{6+}, which resulted in low-cost N-CQDs (QY = 47.5 percent). The developed N-CQDs had a good fluorescence response to the Cr^{6+} target. A good logarithmic correlation (0.3–50 μM) between the fluorescence intensities of the N-CQDs and the Cr^{6+} concentrations was achieved with an R^2 of 0.998 and low LOD of 0.24 μM. This fluorescence sensor demonstrated high repeatability, reproducibility, and stability and completed target detection in <1 min. Through the electrochemical carbonization of sodium citrate and urea,[127] Hou *et al.* proposed a simple, cost-effective, and one-pot approach for the preparation of functionalized fluorescent CQDs with good water solubility. This CQD, which had a QY of 11.9 percent and average dimensions of Ø2.4 nm, was employed as a label-free

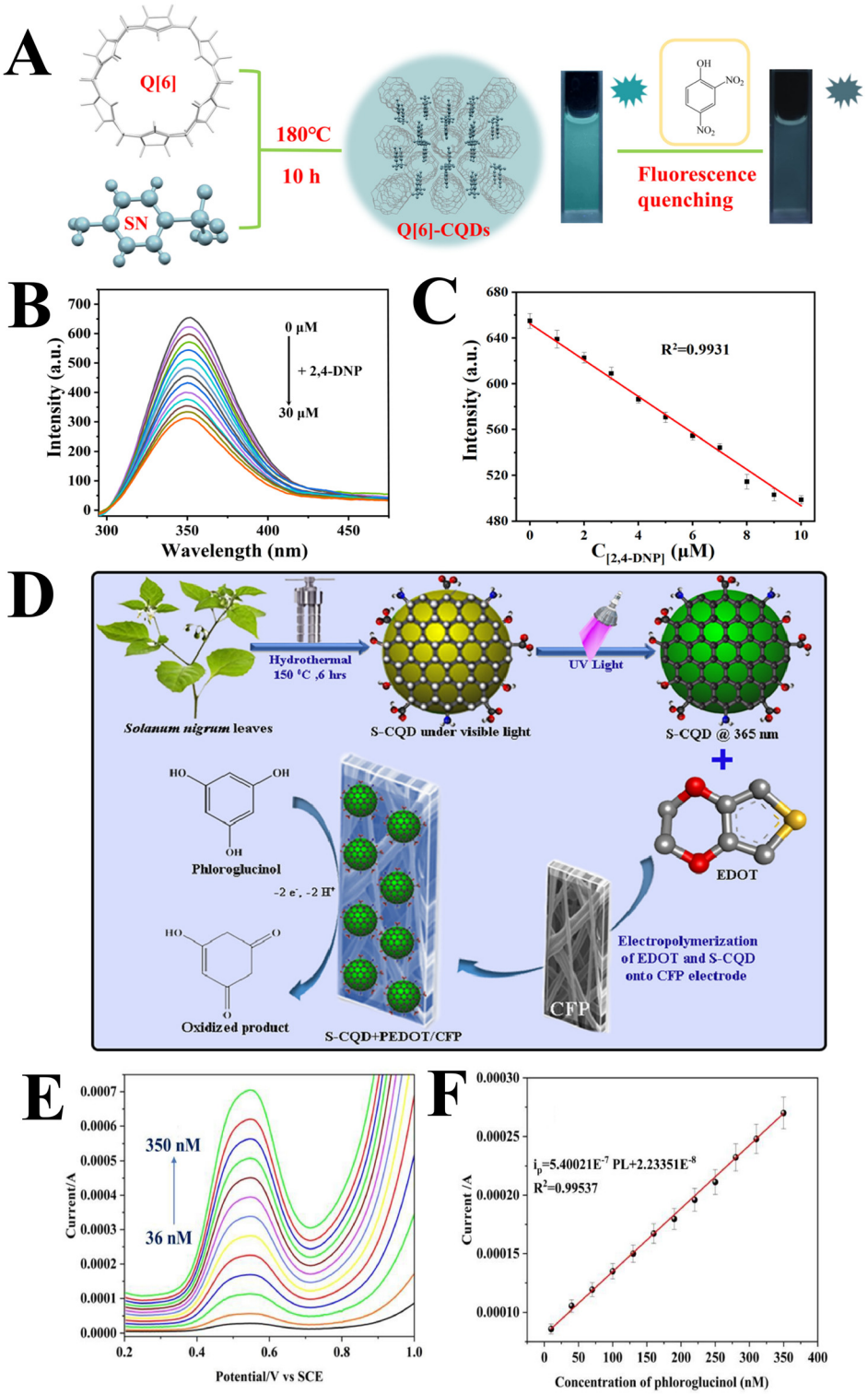

Fig. 8 (A) Hydrothermal synthesis of the Q[6]-CQDs and recognition of 2,4-DNP; (B) detection of 2,4-DNP at different concentrations through the titration fluorescence spectra of the Q[6]-CQDs; (C) associated calibration curve. Reproduced with permission.[114] Copyright 2025, Elsevier; (D) Hydrothermal synthesis of the S-CQD and electro polymerization of the S-CQD + PEDOT/CFP electrode modification for the detection of phloroglucinol; (E) DPV of phloroglucinol at different concentrations; (F) associated calibration curve. Reproduced with permission.[115] Copyright 2023, Elsevier.

sensing probe for the selective detection of Hg^{2+} with a LOD of 3.3 nmol L^{-1}.[128] Further, the easily functionalized surface of CQDs aided in the study and development of fluorescence sensing devices with specialized functions, which expanded practical uses in the detection domain. Due to their high precision and dependability, CQD-based probes have gradually

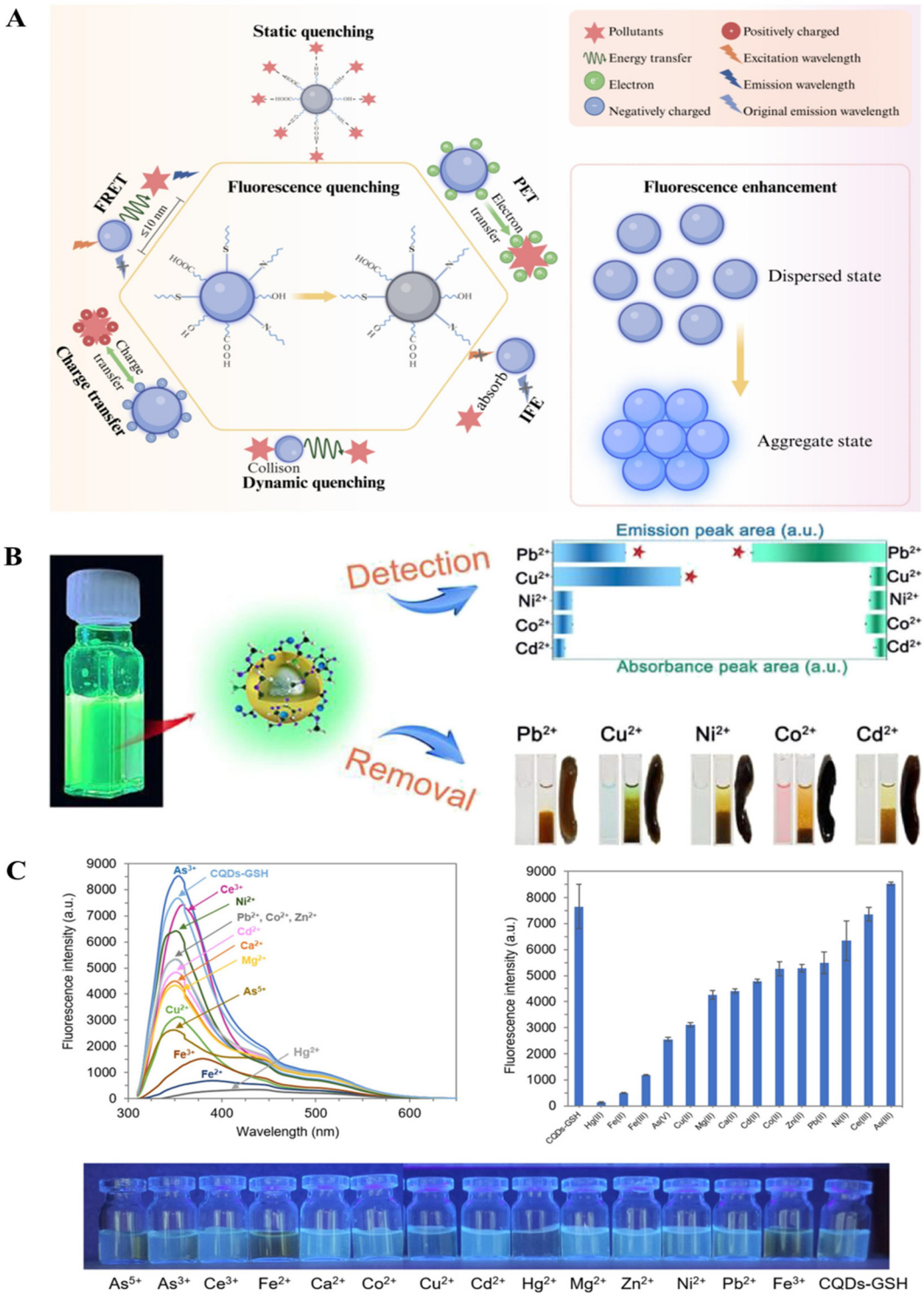

Fig. 9 (A) The mechanisms of fluorescence quenching and fluorescence enhancement in CQDs. Reproduced with permission.[129] Copyright 2025, Elsevier; (B) NCQDs used in the detection and removal of various metals ions. Reproduced with permission.[130] Copyright 2021, American Chemical Society; (C) fluorescence emission spectra, fluorescence intensity (λ_{em} = 355 nm), and photographs under UV illumination at 365 nm of CQDs-GSH (0.2 mg mL^{-1}) in the presence of various metal ions (2.0 mM). Reproduced with permission.[131] Copyright 2025, Elsevier.

become popular sensing devices for the detection of trace concentrations of heavy metal ions.

Fig. 9A shows the fluorescence quenching mechanism of the enhanced CQDs. The fluorescence of CQDs may be quenched through various mechanisms such as static quenching, dynamic quenching, Förster resonance energy transfer (FRET), inner filter effect (IFE), photoinduced electron transfer (PET), and charge transfer. Alternately, it can be enhanced through aggregation-induced emission (AIE).[129] As depicted in Fig. 9B, Nitrogen-doped carbon dots (NCDs) were created through low-temperature thermal sintering, which can simultaneously detect and remove divalent heavy metal ions from water. NCDs are harmless nanoscale entities with sustained fluorescence that are environmentally compatible, which can detect divalent heavy metal ions in ambient waterways. The detection limits for Pb^{2+} and Cu^{2+} were 3 and 15 ppb, respectively. Further, the UV-visible absorbance of NCD spectra may be employed for the dose-dependent analysis of detected Pb^{2+}. Consequently, NCDs can achieve the specific dual goals for the detection of Pb^{2+} *via* spectroscopy, showing that NCD nanoprobes can be employed to determine trace amounts of Pb^{2+} in water.[130] Fig. 9C exhibits the multiple fluorescence detention of various metal ions. The selectivity of CQDs-GSH toward various ions (2.0 mM), including As^{5+}, As^{3+}, Ce^{3+}, Cd^{2+}, Co^{2+}, Ca^{2+}, Mg^{2+}, Ni^{2+}, Cu^{2+}, Pb^{2+}, Zn^{2+}, Hg^{2+}, Fe^{2+}, and Fe^{3+} was evaluated under fluorescence excitation at 300 nm. A significant quenching of the "turn-on" fluorescence emission of CQDs-GSH was observed, specifically in the presence of Hg^{2+}, Fe^{2+}, and Fe^{3+} as indicated by the absence of fluorescence under UV light (365 nm).[131]

3.3.2. Microbial biocontamination. Microbial toxin contamination affects the quality of food and beverages and can cause serious health issues for consumers. The contamination of foods with microbes is possible at any point between harvesting and processing; thus, the monitoring of microbes is an obligatory step. Recent work by Yan *et al.* revealed a novel technique using single color emission CQDs for the rapid detection of Gram-positive bacteria based on the one-step staining of a peptidoglycan layer (the staining remains for 24 h) with a linear range of detection from 50 to 500 μg mL^{-1}.[132] Fig. 10A depicts TEM images of the T-CQDs used for the bacterial detection and confocal images of *S. aureus* and *E. coli* incubated with the T-CQDs.[132] Using a simple hydrothermal treatment with S- or N-containing organic compounds/polymers, sulfur- and nitrogen-doped CQDs (S-CQDs and N-CQDs) were created. Using a qualitative estimation approach, they were tested for their bactericidal activities against Gram-negative (*Escherichia coli*, CECT 831) and Gram-positive (*Bacillus Subtilis* subsp. *subtilis* 168) bacterial strains.

The N-CQDs were found to be more effective than S-CQDs in quantitative tests. The bactericidal activities of these nanomaterials were associated with their unique surface chemistry and nanometric dimensions. In the case of N-CQDs, amides and amines were identified as essential components that facilitated the enhanced bactericidal activities. Electrostatic interactions between their protonated forms and the lipids of bacterial cell membranes translated to the destruction of the bacteria. It was also likely that the capacity of the CQD surfaces to generate oxygen species played an important role. The S-CQDs exhibited significantly lower bactericidal activities than did the N-CQDs, as they possessed a primarily negatively charged surface due to the dissociation of sulfonic/carboxylic groups and sulfates, which limited the growth of Gram-positive bacteria in a size-, rather than chemistry-dependent (electrostatic interactive) manner.

The surfaces of the PCL nanofibers (NFs) were functionalized with CQDs and an aptamer, and a fluorescence intensity recovery was observed upon exposure to *S. aureus* bacteria. Electrospun nanofibers (NFs), with their large surface-area-to-volume ratios enabled effective surface modification, which allowed CQDs to intercalate within the fibers and generate strong fluorescence signals. This design facilitated the development of smart NFs with the capacity for highly sensitive, rapid, and quantitative fluorescence-based detection of *S. aureus* in wounds.[134] A novel magnetic CQD-Fe_3O_4 nanocomposite was developed for the detection of *N*-acyl homoserine lactone (AHL) signaling molecules. *N*-Acyl homoserine lactones (AHLs) are quorum-sensing signaling molecules that allow Gram-negative bacteria to sense their population density and upregulate certain phenotypes, such as virulence factor synthesis, food spoiling, and biofilm formation (Fig. 10B).[133] Various food pathogens such as *Aeromonas hydrophila*, *Pseudomonas aeruginous*, and *Hafina alvei* produce AHL signaling molecules during their growth periods. Both food deterioration and foodborne illnesses are induced by AHL signaling molecules; thus, they can be exploited as common markers for the detection of Gram-negative-based food contamination.[135]

3.3.3. Food additives. Food additives are substances that are added to foods to preserve or improve their safety, freshness, taste, texture, or appearance. For millennia, food additives (*e.g.*, salt in meats like bacon or dried fish), sugar (*e.g.*, in marmalade), and sulfur dioxide (*e.g.*, in wine) have been used to preserve foods.[136,137] These compounds can occur naturally, be manufactured, or be derived from plants, animals, or minerals. They are intentionally added to foods to perform certain technological functions that consumers overlook. Thousands of food additives are used today, with each meant to perform a specific function in making food safer or more appealing. Internationally, there is a permitted threshold for the incorporation of additives in foods. For food monitoring and to ensure that food additives are safe, regular and simple qualitative analyses should be established.[138,139] Employing ammonia as a nitrogen source, a hydrothermal technique was used to synthesize N-CQDs from lemon juice. The electrical characteristics and surface chemical reactivities of CQDs were improved through N-doping, which made them more conducive to chemically interact with Fe^{3+} to create N-GQDs–Fe^{3+}. The N-CQDs that exhibited bright blue fluorescence were employed as novel fluorescent probes for the sensitive and selective detection of Fe^{3+}. Furthermore, the impact of Fe^{3+} ion quenching on the fluorescence of N-CQDs was induced by both dynamic and static quenching mechanisms. This N-CQD-

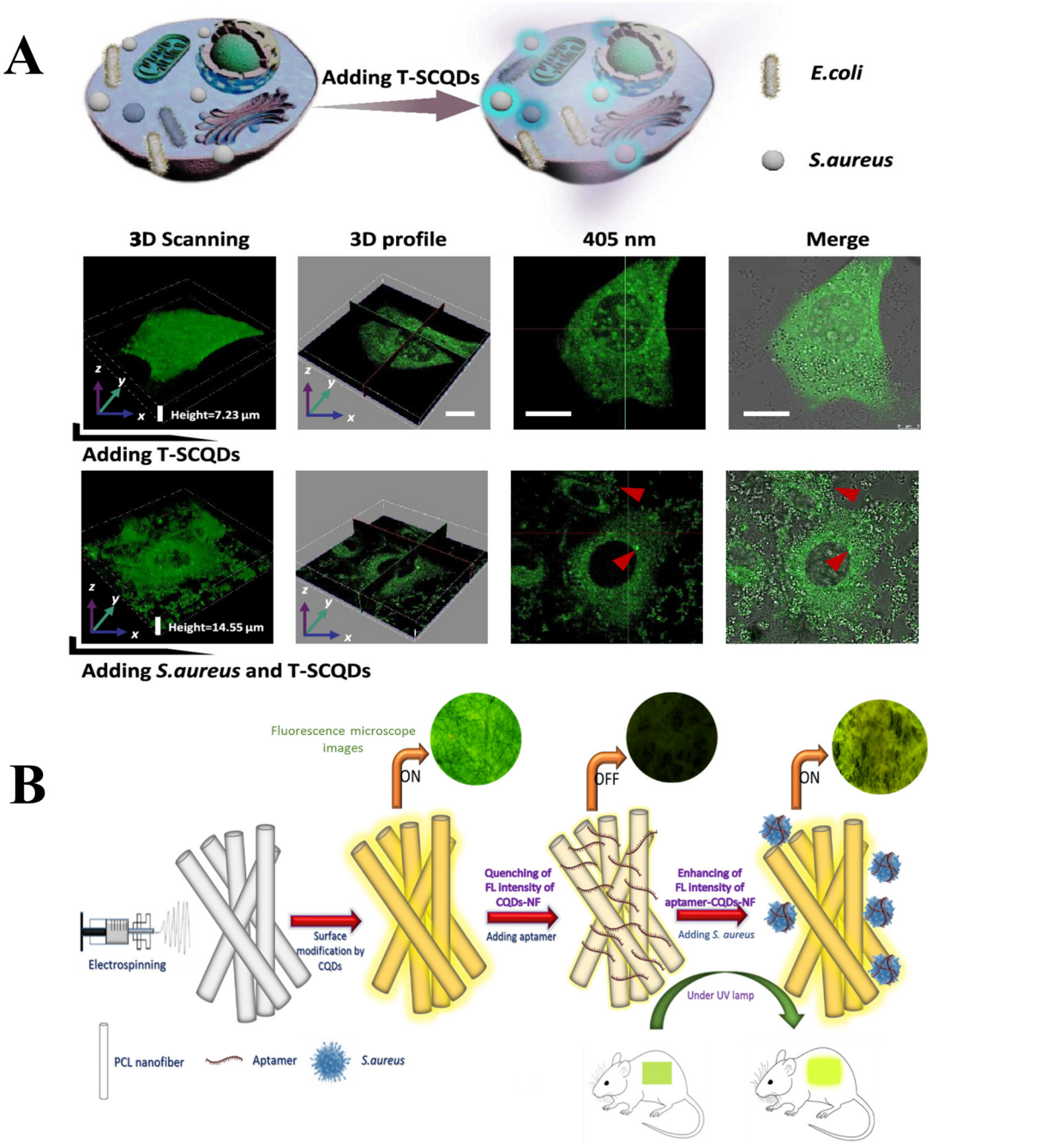

Fig. 10 (A) Scheme of confocal images of *S. aureus* incubated with T-SCQDs (500 μg mL^{-1}) for 24 h; and Confocal images of *S. aureus* following incubation with T-SCQDs (500 μg mL^{-1}) for 24 h, Scale bar: 10 μm. Reproduced with permission.[132] Copyright 2021, American Chemical Society. (B) Surface functionalizes PCL NF with CQDs and aptamer, and the recovery of fluorescence intensity in the presence of *S. aureus* bacteria. Reproduced with permission.[133] Copyright 2022, Elsevier.

based fluorescence sensing system was shown to have interesting applications for the detection of Fe^{3+} in water with several advantages encompassing rapid detection, high sensitivity, strong selectivity, and a wide linear response range with an LOD of 140 ppb.[140] A green CQD sensor was used to selectively and sensitively detect nitrite in the range of from 0.4–20 g mL^{-1}. The detection limit of this novel sensor was determined as 0.23 g mL^{-1} with good recoveries ranging from 86.61 to 103.22%. When nitrite was added at various concentrations, the brightness and color of this green fluorescent probe was altered when illuminated with a portable ultraviolet lamp. The qualitative and semiquantitative analysis of nitrate concentrations was based on visual changes that could be observed with the naked eye. To monitor and decrease the risk of nitrite

overuse in food processing, the developed fluorescent sensor provided an effective, simple, rapid, and low-cost analytical approach for the sensitive and visible detection of nitrites in meat samples. Fluorescent CQDs were used as a chemometric tool to establish a sensing technique in this study.[141] The CQDs were synthesized using natural *Caelsalpinia pulcherrima* seeds *via* a straightforward one-step hydrothermal process, and their chemical structures were further investigated. Five food additives (citric acid, lactic acid, ascorbic acid, sodium benzoate, and potassium sorbate) were sensitively detected with a LOD as low as 252 ng mL^{-1}. Following the optimization of experimental conditions, the sensing platform was created utilizing a supervised approach for the detection of linear discriminant analysis (LDA) patterns, where different quantities of additives were distinguished in pickled olives.[142]

3.4. Determination of pharmaceutical compounds

CQDs are novel types of nano-carbons that are currently preferred over semiconductor quantum dots (QDs) due to their solubility, low toxicity, environmental compatibility, as well as inexpensive and simple manufacturing that provide the required optical properties.[143] Furthermore, specific synthesis pathways were observed to influence their physiochemical properties. CQDs can emit fluorescence over a wide range of wavelengths (ultraviolet (UV) to near-infrared (NIR)), which makes them ideal for pharmaceutical applications. Their excitation wavelengths can be modified to control the fluorescence of these nano-carbon entities. CQDs are currently applied for bioimaging, biosensing, electrochemical biosensing, drug delivery, gene delivery, photodynamic therapies in cancer treatments, pharmaceutical formulations, and inflammatory treatments, among other uses.[144–151]

3.4.1. Antimicrobial drugs. An N-CQD-decorated gadolinium oxide (N-CQD@Gd_2O_3) nanocomposite was hydrothermally synthesized. Rather than a conventional Gd_2O_3 nanorod-like structure, the nanocomposite exhibited a nanoseed-like geometry, which was utilized for the electrochemical analysis of clioquinol (CQL). The developed N-CQD@Gd_2O_3/GCE sensor had a LOD for CQL of 2.1 nM and a high sensitivity of 3.6 MA cm^{-2}.[152] Additionally, it exhibited excellent stability, repeatability, and reproducibility. Another electrochemical sensor design was based on CQDs, ZnO-NFs, and Poly(CTAB) for the simultaneous determination of paracetamol (PAR) and ciprofloxacin (CIP). Due to the high conductivities and large surface areas of the CQDs and ZnO-NFs in conjunction with the synergistic effects of CQD/ZnO-NFs and Poly (CTAB), the CQD/ZnO-NFs/Poly(CTAB)/GCE sensor demonstrated favorable electrochemical parameters. These included an increased current response, well-separated peak potentials, and good linear ranges from 0.05–30.0 μM and 0.01–30.0 μM for PAR and CIP, respectively, with low LODs at 2.47 nM and 1.97 nM, respectively.[153] The use of NCQDs coated with molecularly imprinted polymers (MIPs) was disclosed for a fluorometric test in the detection of doxycycline. The NCQDs were integrated into a molecularly imprinted doxycycline polymer. The fluorescence of the NCQDs was quenched by doxycycline, and the functional groups on the NCQDs surfaces were revealed to play an essential role in quenching efficiency. Due to improved electron transfer from the N-CQDs to the doxycycline, a higher fraction of carboxyl groups on the surfaces of N-CQDs translated to enhanced quenching efficiencies. Doxycycline was specifically and quickly recognized by the N-CQD@MIP composite. The fluorescence decreased linearly under doxycycline concentrations (5 to 50 μM with an 87 nM LOD) and the sensor was used in the electrochemical analysis of doxycycline in spiked pig serum.[154] Dextrose derived CQDs that were produced in a single step were used to modify four different sensors for the detection of gemifloxacin. This sensor revealed linearity under concentrations that ranged from 10^{-6}–10^{-2} M. The LOD for the target medication was traced down to 210 nM levels. Devoid of pretreatment measures, gemifloxacin was successfully identified in pharmaceutical formulations and various water samples were tested with good recovery (96.9–105.3% with SD values of 3).[155] Other work reported on a one-step process for the synthesis of CQDs from biogenic polyamines (PAs) as an antibacterial agent for the treatment of skin resident bacterial keratitis (BK). Furthermore, the CQDs were synthesized through the direct pyrolysis of spermidine (Spd) powder using a simple dry heating process, which had higher solubilities and yields than those made from putrescine or spermine. CQDs derived from Spds (CQDSpds) exhibited antibacterial activities against non-multidrug resistant *Escherichia coli*, *Staphylococcus aureus*, *Pseudomonas aeruginosa*, and *Salmonella enterica serovar*, Enteritidis bacteria, as well as multidrug-resistant *S. aureus* bacteria. The QDSpds exhibited a 2500-fold lower minimal inhibitory concentration (MIC) than spermidine alone, which was indicative of their potent antibacterial properties.[156] Wang *et al.* developed a fluorescence CdTeQDs@SiO_2/N-CDs@MIPs sensor for the detection of tetracycline.[157] The N-CDs detected response signals from tetracycline, CdTeQDs served as reference signals, while the molecularly imprinted polymers (MIPs) served as the recognition element for tetracycline. This fluorescence sensor demonstrated an LOD of 0.846 μM with a linear range of from 0–140 μM, and response time of 1.0 min.[157] Fig. 11A shows the one-step solvothermal synthesis of cyan CQDs (C-CQDs) for lysosome imaging, and the detection of chlortetracycline HCl (CTC), tetracycline HCl (TET), and oxytetracycline HCl (OTC) using 1,5-diaminonapththalene as the precursor.[158] Cell imaging was done to observe the aggregation of C-CQDs and fluorescence colocalization analysis was performed, as well as inhibition experiments, as seen in Fig. 11B. Finally, Fig. 11C displays the emission spectra for the detection of CTC, TET, and OTC at different concentrations with their corresponding calibration curves. The LODs for CTC, TET, OTC were determined to be 0.15 μM, 0.18 μM, and 0.12 μM respectively, which also showed good stability under different temperatures, pH, and ionic environments.[158]

3.4.2. Anticancer drugs. A label-free N-CQD-based nanosensor was developed, enabling the fluorescence activation imaging of Cyt c release during cell death. Quantitative Cyt c measurements were possible due to Cyt c's inner filter action on N-doped

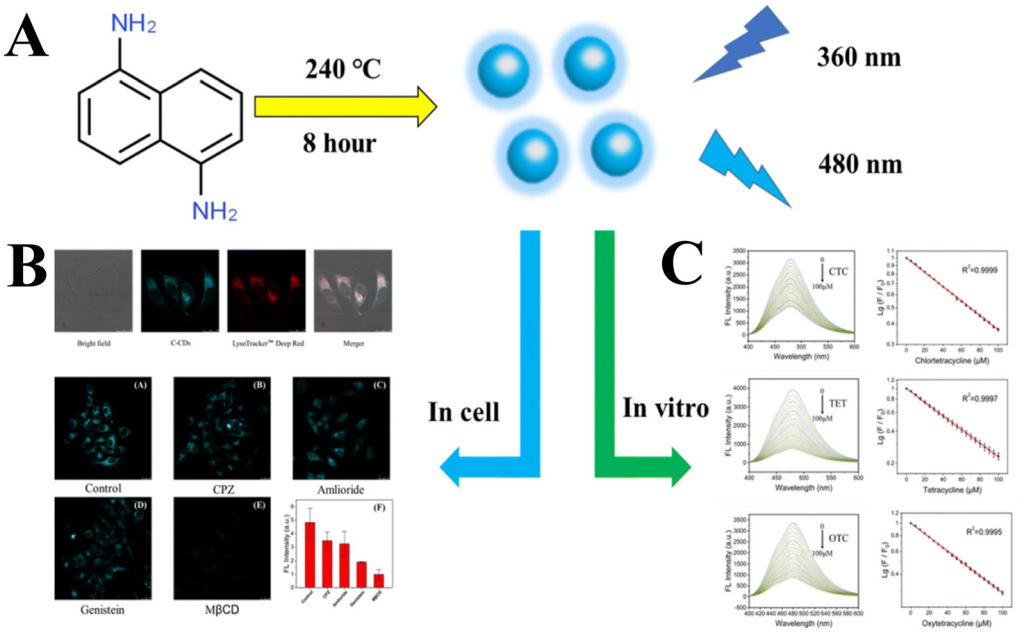

Fig. 11 (A) Schematic diagram of the synthesis of C-CQDs; (B) fluorescence colocalization assay of C-CQDs and in-cell experiments of the C-CQDs with their average fluorescence intensities; (C) emission spectra of the C-CQDs upon the addition of different concentrations of CTC, TET, and OTC, with their respective calibration curves. Reproduced with permission.[158] Copyright 2022, Royal Society of Chemistry.

CQDs. The nanosensor exhibited strong cell-membrane permeability and low cytotoxicity, along with good sensitivity and selectivity. These attributes made possible the *in situ* imaging of Cyt c for apoptosis studies. Moreover, the developed nanosensor was effectively used to monitor the intracellular release of Cyt c and observe Cyt c in zebrafish. It also provided a suitable platform for the screening of apoptosis-inducing chemicals within cells. Due to these advantages and possibilities, the developed assay was important not only for better elucidating specific diseases at the cellular level, but also for apoptotic investigations and screening of anti-cancer therapies during the initial stages of drug development.[159] The N-CQD@Co_3O_4 nanocomposite was synthesized using a simple microwave technique, where the addition of N-CQD enhanced its electrocatalytic activities. This ultrasonication approach was also employed to hybridize the N-CQD@Co_3O_4 nanocomposite with MWCNTs. N-CQDs have a graphitic conjugated structure that allows them to attach to MWCNTs in forming a hybrid nanocomposite. A N-CQD@Co_3O_4/MWCNT hybrid nanocomposite electrode was fabricated and used for the simultaneous determination of flutamide (FLU) and nitrofurantoin (NF). The electrochemical behaviors of FLU and NF on the surface of the proposed sensor were investigated using CV and DPV techniques, which revealed that the hybrid nanocomposite provided a considerable population of reactive sites for FLU and NF redox reactions. The sensor had linear ranges of 0.05–590 μM for FLU and 0.05–1220 μM for NF with LODs of 0.017 μM and 0.044 μM, respectively. Further, the practical applicability of the proposed sensor was tested in human urine samples.[160] In this study the N-CQD doped Fe_2O_3 nanocomposite was synthesized using a hydrothermal technique, and ultrasonication was employed to generate a ternary N-CQD@Fe_2O_3/MWCNT nanocomposite. The graphitic conjugated structure of the N-CQDs created a linkage with MWCNTs, which yielded a stable ternary nanocomposite. The modified ternary N-CQD@Fe_2O_3/MWCNT nanocomposite electrode was then utilized for the simultaneous electrochemical detection of 5-Fluorouracil, uric acid, and Xanthine. For UA, XA, and 5-FU, well-defined electrochemical anodic peaks with peak potential separations of 0.35 V (UA – XA), 0.38 V (XA – 5-FU), and 0.73 V (UA – 5-FU), respectively, were obtained, which were significant enough for the simultaneous detection of the three analytes.[161]

4. Summary and outlook

CQDs are 0D nanomaterials that can initiate positive paradigm shifts across numerous domains of science and technology. Owing to their distinctive features, CQDs are promising for myriad sensing applications. This review highlighted recent advances in CQDs associated with their synthesis, properties, and sensing applications. Various strategies for the synthesis of CQDs, as well as their advantages and limitations in terms of mass production, cost-effectiveness, and availability, were discussed. Many CQD-based sensors for the detection of biomarkers, contaminants, food additives, toxins, pathogens, and drugs discussed in this review article are summarized and compared in Table 1. Factors that should be considered in the design of CQDs and their composites are surface functionalization, active surface areas, dimensions, conductivity, and the morphologies of the materials. Various oxygen-containing functional

Table 1 Comparison of CQD-based sensors for the detection of various analytes in medical diagnoses, environmental monitoring, food safety, and pharmaceutical applications

Materials	Synthesis	Size (nm)	Method	Analyte	Sample	Linear range	Limit of detection	Ref.
Biomarker detection								
AuNPs@GQDs	Hydrothermal	—	EC/GCE	cTnT	Human serum	10–1000 pg mL^{-1}	0.1 pg mL^{-1}	80
Anti CEA/GQDs/Au@Pt	Hydrothermal	—	EC/PWE	CEA	Human serum	0.01–10 ng mL^{-1}	0.006 ng mL^{-1}	94
NGQD@NC@Pd HNS	Pyrolysis	15	EC/GCE	H_2O_2	PBS	0–2500 μM	20 nM	83
N-GQD@SWCNHs	Hydrothermal	4–7	EC/GCE	AFP	Human serum	0.001–200 ng mL^{-1}	0.25 pg mL^{-1}	85
Au-GQDs	Hydrothermal	12.8	EC/GCE	DA	PBS	2–50 μM	840 nM	95
CS/N-GQDs	Microwave	3–4	EC/SPCE	DA	PBS	1–200 μM	145 nM	96
GQDs-eth	Pyrolysis	3–5	EC/GCE	DA	PBS	1–150 μM	115 nM	97
GQDs/CS	Pyrolysis	3	EC/CPE	Epinephrine	PBS	0.36–380 μM	0.3 nM	98
CQDs-CS	Microwave	—	EC/GCE	DA	PBS	0.1–30 μM	11.2 nM	99
CQDs	Pyrolysis	—	EC/CPE	Serotonin	PBS	0.01–8 μM	4 nM	100
GQDs-AuNPs	Pyrolysis	6	EC/GCE	Norepinephrine	PBS	0.5–7.5 μM	150 nM	101
GQDs/IL	Pyrolysis	—	EC/CPE	Norepinephrine	PBS	0.2–400 μM	60 nM	102
MIP/GQDs/2D-hBN/GCE	Pyrolysis	—	EC/GCE	Serotonin	PBS	1×10^{-6}–0.01 μM	0.2 nM	103
GCE/CQDs/CuO	Pyrolysis	—	EC/CPE	Epinephrine	Chicken blood serum	10–100 μM	15.99 μM	165
N-CQD	Pyrolysis	—	Fluorescent	Gabapentin		0.5–80 μg mL^{-1}	0.16 μM	166
N-CQD-MnO_2	Hydrothermal	4.2	Fluorescent	Acetylcholinesterase		1–50 mU	91 mU	167
S-CQDs	Hydrothermal	—	Fluorescent	Acetylcholinesterase/Malathion/Chlorpyrifos		5–330 ppb	1.70, 1.50 ppb	168
Environmental monitoring								
NH_2-GQD@VMSF	Hydrothermal	3.5	EC/ITO	Hg^{2+} Cd^{2+} Cu^{2+}	Human serum	10 pM–1 nM 20 nM–1 μM 10 pM–1 nM	9.8 pM 4.3 pM 8.3 pM	106
GQD	Chemical Oxidation	—	EC/ITO	Hg^{2+}	NaOH	0–500 ppb	10 ppb	110
N-CQDs	Hydrothermal	2–3	PL	4-NP	Tap water	1–200 μM	0.4 μM	91
Cr-CDs	Hydrothermal	4	Fluorescent	4-NP	Human urine	0.8–150 μM	0.27 μM	116
GQDs	Pyrolysis	4–5	EC/GCE	Parathion	PBS	0.01–10^6 ng L^{-1}	46 pg L^{-1}	117
GQD-DPA	Pyrolysis	4–8	EC/GCE	Pb^{2+}	Tap water	0.03–2.8 nM	0.01 nM	118
N-GQDs	Oxidative Ultrasonication	—	EC/GCE	TNT	PBS	1–400 ppb	0.2 ppb	119
CQD	Hydrothermal	—	Fluorescent	Fe^{3+}	PBS	2–50 μM	0.32 μM	164
Pr-CQDs	Solvothermal	—	Fluorescent	Hg^{2+}	Water	0–10 μM	90.3 nM	169
LaCe-CQDs	Hydrothermal	3.27	Fluorescent	Fe^{3+}	Lake water	0–60 μM	0.753 μM	170
B-CQDs N-CQD	Hydrothermal	5–7	Colorimetric	Ag^{+} Ca^{2+}	Tap water	0.06–1.23 μM	0.174 μM 0.391 μM	171
Food safety								
CQDs	Hydrothermal	50	Fluorescent	Oxalate	Tris buffer	1×10^{-5}–7×10^{-5} M	1×10^{-6} M	124
Z-CDs	Pyrolysis	2–6	Fluorescent	EDTA & Zn^{2+}	Tap water	2.5–25 μM & 2–15 μM	0.3 & 0.5 μM	126
B,N-CQDs	Hydrothermal	3.3	Fluorescent	Cr^{6+}	Water	0.3–500 μM	0.24 μM	127
NCDs	Pyrolysis	—	Fluorescent	Pb^{2+} Cu^{2+}	Water	—	3 ppb 15 ppb	130
Fe_3O_4-CQDs	Hydrothermal	5–15	Fluorescent	AHLs	Fish juice and milk	3.65×10^{-3} μmol L^{-1}–0.96×10^{-1} μmol L^{-1}	3.29×10^{-5} μmol L^{-1}	135
N-CQDs	Hydrothermal	—	Fluorescent	Fe^{3+}	Water	1–90 μM	2.5 μM	140
CQDs	Hydrothermal	3.4	Fluorescent	NO_2^-	Water	0.4–20 μg ml^{-1}	0.23 μg ml^{-1}	141
FM-CDs	Hydrothermal	0.5–4.0	Fluorescent	Citric acid	Pickled olives	0.955580–9.148562 μg ml^{-1}	285.490 ng ml^{-1}	142
NSDC-dots	Solvothermal	4.4	Fluorescent	Co^{2+}	Canned tuna	0–0.7 μM	0.012 μM	59

Table 1 *(Contd.)*

Materials	Synthesis	Size (nm)	Method	Analyte	Sample	Linear range	Limit of detection	Ref.
NCQDs	Hydrothermal	7.2	Fluorescent	Hg^{2+}	Grass shrimp	0–5.0 μmol L^{-1}	42.4 nmol L^{-1}	172
N@CQDs	Microwave	1.5	Fluorescent	Allura red	Beverages	0.07–10.0 μg mL^{-1}	0.01 μg mL^{-1}	173
NCQDs	Hydrothermal	2–3	PL	Aspartic acid	PBS	0–100 μl	134.2 nM	174
Pharmaceutical application								
N-CQDs@Gd_2O_3	Hydrothermal	7	EC/GCE	Clioquinol	Serum	0.3–220 μM	2.1 nM	152
N-CQDs/ZnO-NFs	Hydrothermal	5.48	EC/GCE	Paracetamol Ciprofloxacin	Human serum	0.05–30.0 μM 0.01–30.0 μM	2.47 nM 1.97 nM	153
NCQDs@MIP	Hydrothermal	—	EC/GCE	Doxycycline	Pig serum	5–50 μM	87 nM	154
CQDs	Ultrasonic-chemical	10	EC/GCE	Gemifloxacin	Water	10^{-5}–10^{-2} μM	210 nM	155
N,S self-doped CQDs	Hydrothermal	6.5	Fluorescent	Tetracycline	Cancer cells	0.5–47.6 μM	15.6 nM	162
Mannose modified-CQDs	Pyrolysis	3.5	Fluorescent	*E. coli*	Human urine	10^3–10^8 CFU mL^{-1}	450 CFU mL^{-1}	163
P-CQDs	Pyrolysis	2.48	Fluorescent	Tetracycline	Urine sample	0–80 μM	0.120 μM	175
PQDs/CDs@MIP	Hydrothermal	—	Fluorescent	Ciprofloxacin	Prawn-1, Crucian carp	0.01–30.0 μmol L^{-1}	0.005 μmol L^{-1}	176
TOCDs	Pyrolysis	2.63	Fluorescent	Glutathione	Bacteria	2.5–1000 nM	1.5408 nM	177
N-CQDs	Hydrothermal	3.77	Fluorescent	Ciprofloxacin	Bacteria	0.1 to 1 μM	316 nm.	178

Abbreviations: AFP: α-fetoprotein; BN: boron nitride; CD: carbon dot; CEA: carcinoembryonic antigen; CPE: carbon paste electrode; CQD: carbon quantum dot; cTnL: cardiac troponin; CRP: C-reactive protein; CS: chitosan; DA: dopamine; EC: electrochemical method; eth: ethylenediamine; H_2O_2: hydrogen peroxide; IL: ionic liquid; ITO: indium tin oxide, Gd_2O_3: gadolinium oxide; GCE: glassy carbon electrode; GQD: graphene quantum dot; MIP: molecularly imprinted polymer; NIR: near-infrared; 4-NP: 4-nitrophenol; PWE: paper working electrode; SPCE: screen-printed carbon electrode; SPGE: screen-printed gold electrode; TNT: trinitrotoluene; VMSF: vertically ordered mesoporous silica-nanochannel film; ZnO: zinc oxide.

groups exist on the surfaces of CQDs, which facilitate the surface functionalization *via* covalent bonding and hydrogen bonding. Modified CQDs became more catalytically active and led to lower limits of detection and higher sensitivity. The active surface area is another important factor; CQDs with higher active surface areas would enhance the sensitivity when detecting a given analyte. The catalytic activities of QDs are contingent on their dimensions. If the size of a QD is decreased, the quantum confinement effect becomes more prominent, which might also affect the sensitivity of the CQD-based sensor.

Although CQDs have attracted intense research attention, enhancing the selectivity, sensitivity, and resilience of sensor platforms is still critical for practical applications. Further developments are required to expand their scope of functionalities and to improve the stability of CQDs. Although numerous strategies have been devised for the fabrication of CQDs, the lack of efficacious methods for their scalable production with tunable features (*e.g.*, dimensions and crystallinity) has limited their applications in various areas. Previously, researchers have focused on the purity of CQDs, as products such as oligomers or other carbon particles may arise, which might interfere with their purity. Additional impurities could be generated due to reaction precursors if utilizing bottom-up synthesis techniques. These issues, in conjunction with the lower degree of control of CQDs, would limit their broad applications. Although several types of CQDs have been successfully synthesized with high-quality yields, their complex internal structures remain unknown. To understand how the features of CQDs can be tuned, a thorough experimental and theoretical investigation is required that emphasizes their crystallinity, size, morphology, and surface defects. In particular, further research is needed to refine synthetic methodologies and to rigorously demonstrate and validate sensing mechanisms.

In summary, various strategies have been developed for the synthesis of CQDs. Although CQDs are still far from being fully utilized, their numerous attractive properties have enabled applications across diverse fields. Notably, CQD-based sensing has been extensively investigated to address pressing challenges in environmental monitoring, food safety, and healthcare. With the rapid advancements in nanotechnology, nanomedicine, and nanoscience more broadly, it is anticipated that increasingly sophisticated CQDs and their composites will be synthesized to enhance their real-world utility.

Conflicts of interest

The authors have no conflicts of interest.

Data availability

As this is a review article, all figures included have been sourced from published literature with appropriate copyright permissions.

Acknowledgements

This work was supported by a discovery grant from the Natural Sciences and Engineering Research Council of Canada (NSERC RGPIN-2022-04238). A. C. acknowledges the NSERC and the Canada Foundation for Innovation (CFI) for the Tier 1 Canada Research Chair Award in Electrochemistry and Nanoscience.

References

1 N. A. A. Nazri, N. H. Azeman, Y. Luo and A. A. A. Bakar, *Opt. Laser Technol.*, 2021, **139**, 106928.
2 K. Elkabiri, H. Quarrad and L. B. Drissi, *RSC Adv.*, 2025, **15**, 13561.
3 S. Mondal, S. Das, B. Sharma and R. Nayak, *J. Drug Delivery Sci. Technol.*, 2025, **108**, 106896.
4 A. Serag, F. A. Almutairi, M. M. Aldhafeeri, R. M. Alzhrani, M. H. Abduljabbar, R. M. Alnemari, Y. S. Althobaiti and A. H. Almalki, *RSC Adv.*, 2025, **15**, 19468.
5 S. M. Asil and M. Narayan, *Nanoscale Adv.*, 2025, **7**, 1104.
6 J. S. A. Devi, S. M. Anju, G. M. Lekha, R. S. Aparna and S. George, *Nanoscale Horiz.*, 2024, **9**, 1683.
7 Z. Dong and Q. Zhou, *Nanoscale*, 2025, **17**, 9786–9803.
8 X. Yu, J. Liu, Y. Yu, S. Zuo and B. Li, *Carbon*, 2014, **68**, 718–724.
9 K. F. Kayani, D. Ghafoor, S. J. Mohammed and O. B. A. Shatery, *Nanoscale Adv.*, 2025, **7**, 42–59.
10 R. Latif, M. Ahmad, M. Awais, A. Khalid, F. Shahzad, M. F. Umer and M. W. Iqbal, *Nanoscale*, 2024, **16**, 3751–3775.
11 X. T. Zheng, A. Ananthanarayanan, K. Q. Luo and P. Chen, *Small*, 2015, **11**, 1620.
12 L. Bao, Z. L. Zhang, Z. Q. Tian, L. Zhang, C. Liu, Y. Lin, B. Qi and D. W. Pang, *Adv. Mater.*, 2011, **23**, 5801–5806.
13 S. Iravani and R. S. Varma, *Environ. Chem. Lett.*, 2020, **18**, 703–727.
14 F. Bruno, S. Sciortino, G. Buscarino, M. L. Soriano, A. Rios, M. Cannas, F. Gelardi, F. Messina and S. Agnello, *Nanomaterials*, 2021, **11**, 1265.
15 H.-L. Yang, L.-F. Bai, Z.-R. Geng, H. Chen, L.-T. Xu, Y.-C. Xie, W.-J. Liu and J. Yin, *Mater. Today Adv.*, 2023, **18**, 100376.
16 Y. Yang, J. Cui, M. Zheng, C. Hu, S. Tan, Y. Xiao, Q. Yang and Y. Liu, *Chem. Commun.*, 2012, **48**, 380.
17 H. Zhu, X. Wang, Y. Li, Z. Wang, F. Yang and X. Yang, *Chem. Commun.*, 2009, **34**, 5118.
18 K. Hareesh, *RSC Adv.*, 2024, **14**, 23404–23422.
19 M. O. Danilov, S. S. Fomanyuk, G. I. Dovbeshko, O. P. Gnatyuk, I. A. Rusetskyi and G. Ya Kolbasov, *J. Electrochem. Soc.*, 2021, **168**, 44514.
20 M. L. Yola and N. Atar, *J. Electrochem. Soc.*, 2018, **165**, 1.
21 L. Han, D. Ghosh, W. Chen, S. Pradhan, X. Chang and S. Chen, *Chem. Mater.*, 2009, **21**, 13.
22 J. Peng, W. Gao, B. K. Gupta, Z. Liu, R. Romero-Aburto, L. Ge, L. Song, L. B. Alemany, X. Zhan, G. Gao, S. A. Vithayathil, B. A. Kaipparettu, A. A. Marti, T. Hayashi, J. J. Zhu and P. M. Ajayan, *Nano Lett.*, 2012, **12**, 844.
23 Z. A. Qiao, Y. Wang, Y. Gao, H. Li, T. Dai, Y. Liu and Q. Huo, *Chem. Commun.*, 2010, **46**, 8812.
24 Y. Dong, C. Chen, X. Zheng, L. Gao, Z. Cui, H. Yang, C. Guo, Y. Chi and C. M. Li, *J. Mater. Chem.*, 2012, **22**, 8764.
25 M. Wu, J. Zhan, B. Geng, P. He, K. Wu, L. Wang, G. Xu, Z. Li, L. Yin and D. Pan, *Nanoscale*, 2017, **9**, 13195–13202.
26 D. Pan, J. Zhang, Z. Li and M. Wu, *Adv. Mater.*, 2010, **22**, 734.
27 X. Tan, Y. Li, X. Li, S. Zhou, L. Fan and S. Yang, *Chem. Commun.*, 2015, **51**, 2544.
28 Q. Lu, S. Zhou, Y. Zhang, M. Chen, B. Li, H. Wei, D. Zhang, J. Zhang and Q. Liu, *Nanomaterials*, 2020, **10**, 1058.
29 X. Li, H. Wang, Y. Shimizu, A. Pyatenko, K. Kawaguchi and N. Koshizaki, *Chem. Commun.*, 2011, **47**, 932.
30 F. F. Sead, Y. Jadeja, A. Kumar, M. M. Rekha, M. Kundlas, S. Saini, K. K. Joshi and H. Noorizadeh, *Nanoscale Adv.*, 2025, **7**, 3961–3998.
31 L. Zhou, B. He and J. Huang, *Chem. Commun.*, 2013, **49**, 8078.
32 H. Peng and J. Travas-Sejdic, *Chem. Mater.*, 2009, **21**, 5563.
33 W. Meng, X. Bai, B. Wang, Z. Liu, S. Lu and B. Yang, *Energy Environ. Mater.*, 2019, **2**, 172.
34 H. Jiang, X. Geng, S. Li, H. Tu, J. Wang, L. Bao, P. Yang and Y. Wan, *J. Mater. Sci. Technol.*, 2020, **59**, 180.
35 Q. Huang, C. Bao, Q. Wang, C. Dong and H. Guan, *Appl. Surf. Sci.*, 2020, **515**, 145974.
36 S. Mandani, D. Dey, B. Sharma and T. K. Sarma, *Carbon*, 2017, **119**, 569.
37 Z. L. Wu, P. Zhang, M. X. Gao, C. F. Liu, W. Wang, F. Leng and C. Z. Huang, *J. Mater. Chem. B*, 2013, **1**, 2868.
38 J. Ge, Q. Jia, W. Liu, L. Guo, Q. Liu, M. Lan, H. Zhang, X. Meng and P. Wang, *Adv. Mater.*, 2015, **27**, 4169.
39 Z. Peng, C. Ji, Y. Zhou, T. Zhao and R. M. Leblanc, *Appl. Mater. Today*, 2020, **20**, 100677.
40 N. Sahiner, S. S. Suner, M. Sahiner and C. Silan, *J. Fluoresc.*, 2019, **29**, 1191.
41 Y. Liu, N. Xiao, N. Gong, H. Wang, X. Shi, W. Gu and L. Ye, *Carbon*, 2014, **68**, 258–264.
42 J. Schneider, C. J. Reckmeier, Y. Xiong, M. V. Seckendorff, A. S. Susha, P. Kasak and A. L. Rogach, *J. Phys. Chem. C*, 2017, **121**, 2014.
43 S. J. Zhuo, J. Fang, J. Wang and C. Q. Zhu, *Methods Appl. Fluoresc.*, 2019, **8**, 015005.
44 N. R. Devi, T. H. V. Kumar and A. K. Sundramoorthy, *J. Electrochem. Soc.*, 2018, **165**, G3112.
45 Y. Chen, X. Sun, X. Wang, W. Pan, G. Yu and J. Wang, *Spectrochim. Acta, Part A*, 2020, **233**, 118230.
46 F. Wang, S. Pang, L. Wang, Q. Li, M. Kreiter and C. Y. Liu, *Chem. Mater.*, 2010, **22**, 4528.
47 S. Liu, J. Tian, L. Wang, Y. Zhang, X. Qin, Y. Luo, A. M. Asiri, A. O. Al-Youbi and X. Sun, *Adv. Mater.*, 2012, **24**, 2037.

48 H. Zhu, X. Wang, Y. Li, Z. Wang, F. Yang and X. Yang, *Chem. Commun.*, 2012, **34**, 5118.
49 S. J. Zhuo, J. Fang, J. Wang and C. Q. Zhu, *Methods Appl. Fluoresc.*, 2019, **8**, 015005.
50 M. O. Danilov, S. S. Fomanyuk, G. I. Dovbeshko, O. P. Gnatyuk, I. A. Rusetskii, G. Y. Kolbasov and G. G. Yaremchuk, *ECS Trans.*, 2020, **99**, 275.
51 L. Shen, S. Zhou, F. Huang, H. Zhou, H. Zhang, S. Wang and S. Zhou, *Nanotechnology*, 2022, **33**, 115602.
52 S. Ahirwar, S. Mallick and D. Bahadur, *ACS Omega*, 2017, **2**, 8343.
53 C. Qi, H. Wang, A. Yang, X. Wang and J. Xu, *ACS Omega*, 2021, **6**, 32904.
54 Y. Li, J. Gao, Y. Shi, Y. Wang, M. Li, A. Pan, M. Hu and G. Zhang, *Carbon*, 2024, **218**, 118653.
55 X. T. Zheng, A. Ananthanarayanan, K. Q. Luo and P. Chen, *Small*, 2015, **11**, 1620.
56 X. Xu, R. Ray, Y. Gu, H. J. Ploehn, L. Gearheart, K. Raker and W. A. Scrivens, *J. Am. Chem. Soc.*, 2004, **126**, 12736.
57 M. Nazar, M. Hasan, B. Wirjosentono, B. A. Gani and C. E. Nada, *ACS Omega*, 2024, **9**, 20571–20581.
58 W. Li, M. Li, Y. Liu, D. Pan, Z. Li, L. Wang and M. Wu, *ACS Appl. Nano Mater.*, 2018, **1**, 1623.
59 A. B. H. Ali, M. R. Elmasry, Y. A. B. Jardan and M. M. El-Wekil, *RSC Adv.*, 2025, **15**, 6962–6973.
60 T.-H. Huang, Y.-C. Chen, W.-C. Wang, Y.-T. Yen, Y.-P. Tsai and C.-H. Lin, *J. Photochem. Photobiol., A*, 2025, **469**, 116603.
61 S. Kumar, S. K. T. Aziz, O. Girshevitz and G. D. Nessim, *J. Phys. Chem. C*, 2018, **122**, 2343.
62 Y. Yang, J. Cui, M. Zheng, C. Hu, S. Tan, Y. Xiao, Q. Yang and Y. Liu, *Chem. Commun.*, 2012, **48**, 380.
63 Z. C. Yang, M. Wang, A. M. Yong, S. Y. Wong, X. H. Zhang, H. Tan, A. Y. Chang, X. Li and J. Wang, *Chem. Commun.*, 2011, **47**, 11615.
64 S. Zhu, Q. Meng, L. Wang, J. Zhang, Y. Song, H. Jin, K. Zhang, H. Sun, H. Wang and B. Yang, *Angew. Chem., Int. Ed.*, 2013, **52**, 3953.
65 S. Sahu, B. Behera, T. K. Maiti and S. Mohapatra, *Chem. Commun.*, 2012, **48**, 8835.
66 B. De and N. A. Karak, *RSC Adv.*, 2013, **3**, 8286.
67 Q. Tang, W. Zhu, B. He and P. Yang, *ACS Nano*, 2017, **11**, 1540.
68 M. L. Liu, B. B. Chen, C. M. Li and C. Z. Huang, *Sci. China: Chem.*, 2019, **62**, 968.
69 A. Halder, M. G. Gallardo, J. Ashley, X. Feng, T. Zhou, L. H. Rigau and Y. Sun, *ACS Appl. Bio Mater.*, 2018, **1**, 452.
70 C. B. Ma, Z. T. Zhu, H. X. Wang, X. Huang, X. Zhang, X. Qi, H. L. Zhang, Y. Zhu, X. Deng, Y. Peng, Y. Han and H. A. Zhang, *Nanoscale*, 2015, **7**, 10162.
71 L. Fan, M. Zhu, X. Lee, R. Zhang, K. Wang, J. Wei, M. Zhong, D. Wu and H. Zhu, *Part. Part. Syst. Charact.*, 2013, **30**, 764.
72 Y. Wang, M. Myers and J. A. Staser, *J. Electrochem. Soc.*, 2018, **165**, 122–130.
73 M. N. Lassere, *Stat. Methods Med. Res.*, 2008, **17**, 303.
74 F. Mollarasouli, K. Asadpour-Zeynali, S. Campuzano, P. Yáñez-Sedeño and J. M. Pingarrón, *Electrochim. Acta*, 2017, **246**, 303–314.
75 T. C. Canevari, M. Nakamura, F. H. Cincotto, F. M. de-Melo and H. E. Toma, *Electrochim. Acta*, 2016, **209**, 464–470.
76 T.-T. D. Pham, L. M. T. Phan, J. Park and S. Cho, *J. Electrochem. Soc.*, 2022, **169**, 8.
77 S. Durairaj, B. Sidhureddy and A. Chen, *J. Electrochem. Soc.*, 2020, **167**, 167511.
78 Z. Altintas, W. M. Fakanya and I. E. Tothill, *Talanta*, 2014, **128**, 177.
79 A. Chen and S. Chatterjee, *Chem. Soc. Rev.*, 2013, **42**, 5425.
80 S. E. Kim, J. C. Yoon, A. Muthurasu and H. Y. Kim, *Langmuir*, 2024, **40**, 25051–25060.
81 H. W. Yang, C. W. Lin, M. Y. Hua, S. S. Liao, Y. T. Chen, H. C. Chen, W. H. Weng, C. K. Chuang, S. T. Pang and C. C. M. Ma, *Adv. Mater.*, 2014, **26**, 3662.
82 S. C. Shah, V. Kayamba, R. M. Peek and D. Heimburger, *J. Global Oncol.*, 2019, **5**, 1–10.
83 J. Xi, C. Xie, Y. Zhang, L. Wang, J. Xiao, X. Duan, J. Ren, F. Xiao and S. Wang, *ACS Appl. Mater. Interfaces*, 2016, **8**, 22563.
84 D. Kurniawan, R. C. Jhang, K. K. Ostrikov and W. H. Chiang, *ACS Appl. Mater. Interfaces*, 2021, **13**, 34572.
85 K. Dutta, S. De, B. Das, S. Bera, B. Guria, M. S. Ali and D. Chattopadhyay, *ACS Biomater. Sci. Eng.*, 2021, **7**, 5541.
86 J. W. Heinecke, *Nat. Chem. Biol.*, 2006, **2**, 300.
87 J. Korram, A. C. Anbalagan, A. Banerjee and S. N. Sawant, *J. Mater. Chem. B*, 2024, **12**, 742–751.
88 J. Korram, P. Koyande, S. Mehetre and S. N. Sawant, *ACS Omega*, 2023, **8**, 31410–31418.
89 H. Hennessey, N. Afara, S. Omanovic and A. L. Padjen, *Anal. Chim. Acta*, 2009, **643**, 45.
90 C. Kokkinos, M. Prodromidis, A. Economou, P. Petrou and S. Kakabakos, *Anal. Chim. Acta*, 2015, **886**, 29.
91 P. Kumar, N. Nesakumar, S. Vedantham and J. B. B. Rayappan, *RSC Adv.*, 2025, **15**, 475–14384.
92 Z. Liu, Y. Gong and Z. A. Fan, *New J. Chem.*, 2016, **40**, 8911.
93 A. Muthumariyappan, U. Rajaji, S. M. Chen, T. W. Chen, Y. L. Li and R. J. Ramalingam, *Ultrason. Sonochem.*, 2019, **57**, 233.
94 L. Li, W. Li, H. Yang, S. Ge and J. Wu, *Sens. Actuators, B*, 2014, **314**, 202.
95 H. S. Jang, D. Kim, C. Lee, B. Yan, X. Qin and Y. Piao, *Inorg. Chem. Commun.*, 2019, **105**, 174.
96 S. B. Aoun, *R. Soc. Open Sci.*, 2017, **4**, 11.
97 Y. Li, Y. Jiang, T. Mo, H. Zhou, Y. Li and S. Li, *J. Electroanal. Chem.*, 2016, **767**, 84.
98 J. Tashkhourian, S. F. Nami-Ana and M. Shamsipur, *J. Mol. Liq.*, 2018, **266**, 548.
99 Q. Huang, S. Hu, H. Zhang, J. Chen, Y. He, F. Li, W. Weng, J. Ni, X. Bao and Y. Lin, *Analyst*, 2013, **138**, 5417.
100 S. S. Shankar, R. M. Shereema, V. Ramachandran, T. V. Sruthi, V. B. S. Kumar and R. B. Rakhi, *ACS Omega*, 2019, **4**, 7903.

101 A. Fajardo, D. Tapia, J. Pizarro, R. Segura and P. Jara, *J. Appl. Electrochem.*, 2018, **49**, 423.
102 P. M. Jahani, M. Jafari, V. K. Gupta and V. K. S. Agarwal, *Int. J. Electrochem. Sci.*, 2020, **15**, 947.
103 M. L. Yola and N. Atar, *Appl. Surf. Sci.*, 2018, **458**, 648–655.
104 D. Ren, X. Wang, C. Leng, W. Meng, J. Zhang and C. A. Han, *J. Electrochem. Soc.*, 2022, **169**, 9.
105 T. T. T. Toan and D. M. Nguyen, *ECS Sens. Plus5*, 2022, **1**, 031603.
106 L. Lu, L. Zhou, J. Chen, F. Yan, J. Liu, X. Dong, F. Xi and P. Chen, *ACS Nano*, 2018, **12**, 12673.
107 C. Tian, Y. Lee, Y. Song, M. R. Elmasry, M. Yoon, D.-H. Kim and S.-Y. Cho, *ACS Appl. Nano Mater.*, 2024, **7**, 5576–5586.
108 T. Vyas and A. Joshi, *Analyst*, 2024, **149**, 1297–1309.
109 C. C. Fu, C. Hsieh, R. S. Juang, S. Gu, G. Ashraf, Y. R. E. Kelly and K. D. Kihm, *J. Mol. Liq.*, 2020, **302**, 1125593.
110 S. L. Ting, S. J. Ee, A. Ananthanarayanan, K. C. Leong and P. Chen, *Electrochim. Acta*, 2015, **172**, 7.
111 S. A. Hira, M. Nallal and K. H. Park, *Sens. Actuators, B*, 2019, **298**, 126861.
112 S. A. Hira, H. S. Hui, Y. Mohammad and K. H. Park, *Catal. Commun.*, 2020, **141**, 106011.
113 D. Das and R. K. Dutta, *ACS Appl. Nano Mater.*, 2021, **4**, 3444.
114 X. Chen, S. Yuan, Y. Ye, X. Yang, X. Xiao and P. Ma, *J. Mol. Struct.*, 2025, **1320**, 139731.
115 P. Keerthana, A. George, L. Benny and A. Varghese, *Electrochim. Acta*, 2023, **448**, 142184.
116 C. Li, Y. Zheng, H. Ding, H. Jiang and X. Wang, *Microchim. Acta*, 2019, **186**, 384.
117 J. Mehta, N. Bhardwaj, S. K. Bhardwaj, S. K. Tuteja, P. Vinayak, A. K. Paul, K. H. Kim and A. Deep, *Anal. Biochem.*, 2017, **523**, 1.
118 M. Hadidi, F. Ahour and S. Keshipour, *J. Iran. Chem. Soc.*, 2022, **19**, 1179.
119 Z. Cai, F. Li, P. Wu, L. Ji, H. Zhang, C. Cai and D. F. Gervasio, *Anal. Chem.*, 2015, **87**, 11803.
120 Z. Liu, V. S. Manikandan and A. Chen, *Curr. Opin. Electrochem.*, 2019, **16**, 127.
121 F. R. Mansour, M. A. A. Hamid, A. Gamal and S. H. Elagamy, *J. Food Compos. Anal.*, 2024, **127**, 105972.
122 X. Shi, W. Wei, Z. Fu, W. Gao, C. Zhang, Q. Zhao, F. Deng and X. Lu, *Talanta*, 2019, **194**, 809.
123 P. Devi, P. Rajput, A. Thakur, K. H. Kim and P. Kumar, *Trends Anal. Chem.*, 2019, **114**, 171.
124 S. Zhang, Q. Wang, G. Tian and H. Ge, *Mater. Lett.*, 2014, **115**, 233.
125 Y. Liu, Y. Zhao and Y. Zhang, *Sens. Actuators, B*, 2014, **196**, 647.
126 M. Yang, Q. Tang, Y. Meng, J. Liu, T. Feng, X. Zhao, S. Zhu, W. Yu and B. Yang, *Langmuir*, 2018, **34**, 7767.
127 Y. Wang, X. Hu, W. Li, X. Huang, Z. Li, W. Zhang, X. Zhang, X. Zou and J. Shi, *Spectrochim. Acta, Part A*, 2020, **243**, 118807.
128 X. Hou, Y. Zhang, H. Wang, Y. Li, L. Wu and G. Zhuang, *Nanoscale*, 2015, **7**, 69–74.
129 F. Wang, Y. Zhang, H. Li, W. Gong, J. Han, S. Jiang, D. Li and Z. Yao, *Food Chem.*, 2025, **463**, 141122.
130 X. C. Yang, Y. L. Yang, M. M. Xu, S. S. Liang, X. L. Pu, J. F. Hu, Q. L. Li, J. T. Zhao and Z. J. Zhang, *ACS Appl. Nano Mater.*, 2021, **4**, 13986.
131 V. Chobpattana, T. Sangtawesin, P. Khaopueak and K. Wechakorn, *Mater. Sci. Eng., B*, 2025, **313**, 117956.
132 C. Yan, C. Wang, T. Hou, P. Guan, Y. Qiao, L. Guo, Y. Teng, X. Hu and H. Wu, *ACS Appl. Mater. Interfaces*, 2021, **13**, 1277.
133 A. B. Pebdeni, M. Hosseini and A. Barkhordari, *Talanta*, 2022, **246**, 123454.
134 N. A. Travlou, D. A. Giannakoudakis, M. Algarra, A. M. Labella, E. Rodríguez-Castellón and T. J. Bandosz, *Carbon*, 2018, **135**, 104.
135 Z. Cui, Z. Li, Y. Jin, T. Ren, J. Chen, X. Wang, K. Zhong, L. Tang, Y. Tang and M. Cao, *Food Chem.*, 2020, **328**, 127063.
136 V. S. Manikandan, Z. Liu and A. Chen, *J. Electroanal. Chem.*, 2018, **819**, 524.
137 M. Govindhan, B. R. Adhikari and A. Chen, *RSC Adv.*, 2014, **4**, 63741.
138 L. Li, M. Zhang and W. Chen, *J. Food Drug Anal.*, 2020, **28**, 641.
139 N. Ngafwan, H. Rasyid, E. S. Abood, W. Kamal Abdelbasset, S. G. Al-Shawi, D. Bokov and A. T. Jalil, *Food Sci. Technol.*, 2021, **42**, e37821.
140 T. K. Mondal, A. Gupta, B. K. Shaw, S. Mondal, U. K. Ghorai and S. K. Saha, *RSC Adv.*, 2016, **6**, 59927.
141 X. Yue, Z. Zhou, Y. Wu, M. Jie, Y. Li, H. Guo and Y. Bai, *New J. Chem.*, 2020, **44**, 8503.
142 S. V. Carneiro, M. H. B. Holanda, H. O. Cunha, J. J. P. Oliveira, S. M. A. Pontes, A. A. C. Cruz, L. M. U. D. Fechine, T. A. Moura, A. R. Paschoal, R. A. Zambelli, R. M. Freire and P. B. A. J. Fechine, *J. Photochem. Photobiol., A*, 2021, **411**, 113198.
143 T. Alomar, N. AlMasoud and F. R. Mansour, *Spectrochim. Acta, Part A*, 2024, **322**, 124825.
144 N. Mohamed, M. Hamed, F. R. Mansour, W. Zarad, S. Emara and A. Shawky, *Luminescence*, 2025, **40**, 1–13.
145 A. H. Kamal, R. E. Kannouma, M. A. Hammad and F. R. Mansour, *Microchem. J.*, 2024, **206**, 111488.
146 D. L. Glasco, A. Sheelam, N. H. B. Ho, A. M Mamaril, M. King and J. G Bell, *ECS Sens. Plus*, 2022, **1**, 010602.
147 A. Gorska, M. Zambrzycki, B. Paczosa-Bator and R. J. Piech, *J. Electrochem. Soc.*, 2022, **169**, 096503.
148 V. Buk, M. E Pemble and K. Twomey, *Electrochim. Acta*, 2019, **293**, 307.
149 S. Singh, J. Wang and S. Cinti, *ECS Sens. Plus*, 2022, **1**, 023401.
150 A. P. F. Turner, *ECS Sens. Plus*, 2022, **1**, 011601.
151 L. Qian, S. Durairaj, S Prins and A. Chen, *Biosens. Bioelectron.*, 2021, **175**, 112836.

152 R. K. Devi, M. Ganesan, T. W. Chen, S. M. Chen, X. Liu, M. A. Ali, S. M. Almutairi and M. Sethupathi, *New J. Chem.*, 2022, **46**, 4090.
153 B. Hatamluyi, F. M. Zahed, Z. Es'haghi and M. Darroudi, *Electroanalysis*, 2020, **32**, 1818.
154 X. Feng, J. Ashley, T. Zhou and Y. Sun, *Microchim. Acta*, 2018, **185**, 500–509.
155 M. F. Ayad, Y. A. Trabik, M. H. Abdelrahman, N. V. Fares and N. Magdy, *Chemosensors*, 2021, **9**, 8.
156 H. J. Jian, R. S. Wu, T. Y. Lin, Y. J. Li, H. J. Lin, S. G. Harroun, J. Y. Lai and C. C. Huang, *ACS Nano*, 2017, **11**, 6703–6716.
157 J. Wang, Y. Qin, Y. Ma, M. Meng and Y. Xu, *Molecules*, 2024, **29**, 5888.
158 T. Zhu, L. Cao, X. Kou, Y. Liu, W.-F. Dong, M. Ge and L. Li, *RSC Adv.*, 2022, **12**, 33761–33771.
159 H. Zhang, B. Zhang, C. Di, M. C. Ali, J. Chen, Z. Li, J. Si, H. Zhang and H. Qiu, *Nanoscale*, 2018, **10**, 5342.
160 G. Muthusankar, R. K. Devi and G. Gopu, *Biosens. Bioelectron.*, 2020, **150**, 111947.
161 M. Ganesan, K. D. Ramadhass and H. C. Chuang, *J. Mol. Liq.*, 2021, **331**, 115768.
162 C. Shi, H. Qi, R. Ma, Z. Sun, L. Xiao, G. Wei, Z. Huang, S. Liu, J. Li, M. Dong, J. Fan and Z. Guo, *Mater. Sci. Eng., C*, 2019, **105**, 110132.
163 C. I. Weng, H. T. Chang, C. H. Lin, Y. W. Shen, B. Unnikrishnan, Y. J. Li and C. C. Huang, *Biosens. Bioelectron.*, 2015, **68**, 6.
164 M. Zhou, Z. Zhou, A. Gong, Y. Zhang and Q. Li, *Talanta*, 2015, **143**, 107.
165 H. Li, C. Sun, R. Vijayaraghavan, F. Zhou, X. Zhang and D. R. MacFarlane, *Carbon*, 2016, **104**, 33.
166 A. H. Almalki, A. H. Abdelazim, M. E. Alosaimi, M. H. Abduljabbar, R. M. Alnemari, A. K. Bamaga and A. Serag, *RSC Adv.*, 2024, **14**, 4089.
167 L. Dewangan, J. Korram, I. Karbhal, R. Nagwanshi and M. L. Satnami, *ACS Appl. Nano Mater.*, 2021, **4**(12), 13612–13624.
168 N. Mahmoudi, F. Fatemi, M. Rahmandoust, F. Mirzajani and S. O. R. Siadat, *Heliyon*, 2023, **9**, e19551.
169 S. Mohandoss, A. Priyadharshini, K. S. Velu, A. A. Napoleon, P. Roy, N. Ahmad, M. R. Khan, S. Palanisamy, S. You and S. Kim, *Mater. Sci. Eng., B*, 2025, **317**, 118236.
170 B. Li, F. Wu, Z. Xie, X. Kang, Y. Wang, W. Li and X. Hu, *Spectrochim. Acta, Part A*, 2025, **327**, 125403.
171 A. Aygün, I. Cobas, R. N. E. Tiri and F. Şen, *RSC Adv.*, 2024, **14**, 10814–10825.
172 D. Shan, H. Yu, Z. Yang, H. Li, R. Jia and Y. Zhang, *Food Chem.*, 2025, **463**, 141308.
173 B. I. Salman, *J. Fluoresc.*, 2024, **34**, 599–608.
174 K. S. Raju, G. S. Das and K. M. Tripathi, *RSC Sustainability*, 2024, **2**, 223–232.
175 C. Wang, Z. Ma, Z. Yao, P. Li, J. Zhang, W. Zhang, X. Zhao and H. Shi, *Phys. Scr.*, 2025, **100**, 055926.
176 Q. Zhang, X. Li, Y. Xu, Z. Xu and L. Xu, *J. Hazard. Mater.*, 2025, **490**, 137845.
177 L. Wu, H. Xiao, J. Xue, X. Lin, Z. Zhu, A. Liu and L. Lin, *Anal. Chim. Acta*, 2025, **1355**, 343983.
178 F. Shen, Z. Lu, K. Yan, K. Luo, S. Pei and P. Xiang, *Sci. Rep.*, 2025, **15**, 28535.